TÉCNICO LISBOA

Radiation environment and effects in human spaceflight: A Lunar Mission

João Tiago Duarte Sabino

Dissertação para a obtenção de Grau de Mestre em

Engenharia Física e Tecnológica

Júri

Presidente:	Professor Mário João Martins Pimenta
Orientador:	Professora Patrícia Carla Serrano Gonçalves
Co-orientador:	Doutora Ana Oliveira Braga Keating
Vogais:	Professor Pedro Miguel Félix Brogueira

Novembro 2012

Acknowledgments

Despite being an individual work this thesis could not have been written if it were not for the help of many to whom I would like to express my sincere gratitude:

- I would like to start by thanking my supervisor Professora Patrícia Gonçalves for all her help specially during the last stretch in preparing this document and for giving me the opportunity to work in space engineering at LIP.
- Ana Keating, for her precious help in the revision of this document and for the insightful advices even being at a distance.
- Bernardo Tomé, who is always in a good mood and ready to help, not fearing my messiest C++ codes.
- All the friends who accompanied me during these work, for making my work and studies easier with the so needed breaks, for the good times spent together and for giving me courage when I started to feel down.
- My family, for all their support, specially Ana and Vitor. It is good to know that there is always someone ready to back me up, no matter what.
- Maria, to whom I will still be thanking long after we become wrinkled and grey.

Resumo

Este trabalho contém uma revisão das quantidades e conceitos usados para descrever o ambiente de radiação a que uma tripulação está sujeita no âmbito de uma missão lunar. São abordados os efeitos da radiação em tecidos biológicos e as suas consequências para a saúde do astronauta. O ambiente de radiação é descrito com base em dados simulados com o software CREME e também utilizando dados das medições de neutrões do albedo lunar obtidos pela sonda Lunar Prospector. A missão é dividida em cinco fases correspondentes a partes da trajetória da nave: LEO (Low Earth Orbit), travessia das cinturas de Van Allen, GEO (Geosynchronous Earth Orbit), órbita da Lua e superfície da Lua. Foi desenvolvida uma aplicação em Geant4 para simular os efeitos da radiação nas tripulações ao longo de toda a missão. A ferramenta de simulação Geant4, que permite simular o transporte e as interacções das partículas através da matéria, é utilizada neste trabalho para avaliar os espectros e tipos de partículas que mais afectam os astronautas, assim como quantidades dosimétricas relevantes. Estas quantidades são avaliadas para condições de mínimo solar e máximo solar tendo em conta possíveis erupções solares.

Palavras-chave: espaço, radiação, lua, geant4, fluência, dose.

Abstract

This work contains an overview of the radiation physics quantities and concepts that are of concern in a crewed mission to the Moon. The radiation effects in biological tissue and their consequences for the astronaut health are addressed. The environment scenario of a mission to the Moon is simulated based on data obtained with the software CREME and data from the Lunar Lander neutron measurements. The mission is divided in five phases concerning the different stages of the trajectory of the mission: LEO, VAB traversing, GEO, Moon orbit, and Moon surface. Major details on the development of a software application in Geant 4 are presented. The application is used for the transport of radiation particles through matter, to simulate the physics processes involved, and to obtain the resultant absorbed dose, equivalent dose and spectre of secondary particles. These quantities are evaluated for solar minimum and solar maximum conditions, the possible occurence of solar flares is also considered.

Keywords: space, radiation, moon, geant4, fluence, dose.

Contents

List of Tables

List of Figures

Nomenclature

Acronyms

BFO	Blood forming organs.
CME	Coronal Mass Ejection
ESA	European Space Agency
EVA	Extravehicular Activity
GCR	Galactic Cosmic Rays
GEO	Geosynchronous Earth Orbit
ICRP	International Comission on Radiological Protection
ICRU	International Commission on Radiation Units and Measurements
IS	International System of Units
ISRO	Indian Space Research Organisation
ISS	International Space Station
LEO	Low Earth Orbit - any orbit below 2000 km of altitude.
LET	Linear Energy Transfer
LLO	Low Lunar Orbit
NASA	United States National Aeronautics and Space Administration.
NCRP	National Council for Radiological Protection
PEL	Permissible exposure limit.
SAA	South Atlantic Anomaly
SEP	Solar energetic particles event
SF	Solar Flare

SRES Space Radiation Effects Simulator

SRF Acronym I use to designate the lunar surface mission phase

TLI Trans Lunar Injection

VAB Van Allen radiation belts

Chapter 1

Introduction

"Human exploration beyond low Earth orbit has become the major global focus for human spaceflight activities, with the Moon being the first key stepping stone in these activities." ESA

1.1 Motivation

In December 2005 United States National Aeronautics and Space Administration (NASA) works began on the Constellation Program to send astronauts first to the International Space Station (ISS), then to the Moon (where a permanent outpost would be built) and eventually to Mars. The program was cancelled in 2010 due to budget restrictions and replaced by the U.S. National Space Policy that aims the completion of the design of a new heavy-lift launch vehicle by 2015 and to begin its construction thereafter. The new policy also provides a U.S. crewed orbital Mars mission by the mid-2030s, preceded by an asteroid mission by 2025. Once being met, this objectives represent an enormous technological and scientific achievement, however, putting aside possible budget restrictions, there are still several important obstacles to overcome [1].

Three factors affecting long-duration human space exploration are of central importance, yet do not lend themselves to definitive assessment based on the presently available data: (1) the effects of prolonged exposure to solar and galactic cosmic rays on the human body; (2) the impact on humans of prolonged periods of weightlessness followed by a sudden need to function, without assistance, in a relatively strong gravitational field (i.e. Mars); and (3) the psychological effects on individuals facing demanding tasks in extreme isolation for well over year with no possibility for direct outside human intervention [2].

The radiation environment in the solar system presents the main constrain to human spaceflight outside Earth's protecting radiation belts. As the human presence in space tends to increase or the will to reach other planets grows, radiation in space becomes a more compelling obstacle that needs to be dealt with.

The risks that radiation exposure present to space missions affect directly the mission planing. For this reason, a good knowledge of the radiation environment in all mission phases is essential. Therefore,

the development of reliable prediction tools is of major importance to assist mission planing and assure minimum levels of safety for the crew. This work aims at analysing the different factors to be taken into account to acurately predict the effects of space radiation to human spaceflight. In order to fulfill this goal a simulation software tool, named Space Radiation Effects Simulator (SRES), was developed. SRES will provide educated guesses of the effects of radiation expected under certain conditions. The SRES development is described in this work and the results for simulations, assuming a real lunar mission scenario, are presented.

1.2 Background in Human Spaceflight

The first human to leave the confines of the Earth and ascend into space was the Russian cosmonaut Yuri Gagarin (1934–1968), on 12 April 1961. On December 1968, the Apollo 8 was the first mission beyond low Earth orbit (LEO) carrying a crew of three individuals. Less than one year later, on July 21 of 1969, Apollo 11 landed on the moon and Niel Armstrong (1930-2012) became the first man who walked on it. Since 31 October 2000, humans have been present in space without interruption in the International Space Station. Presently 528 individuals from 38 countries have been in space but of this 528 astronauts, just 24 traveled beyond low Earth orbit and only 12 walked on the Moon [3]. Quite surprisingly, the last manned mission to the moon was about 40 years ago, during the Apollo 17 mission, on December 11 of 1972, and, apart from the twenty-four astronauts who visited the Moon, during the Apollo missions between 1968 and 1972, no human being has gone beyond low Earth orbit again.

However, robotic space exploration beyond LEO hasn't come to an halt. Instead, it rather increased over time as well as the participation of an ever increasing number of different countries. Satellites have been sent not only to the moon but also to more distant objects like Mercury, Venus, Mars and even the asteroid Eros. Focusing on the moon, some recent data is available from probes such as the Chandrayaan-1 [4], the Lunar Prospector [5] and the Lunar Reconnaissance Orbiter [6]. Also, new robotic missions to the moon are in development such as the Chandrayyaan-2, of the Indian Space Research Organisation (ISRO) [7], proposed to be launched in 2013, and the Lunar Lander, of the European Space Agency (ESA), that aims to land in a strategic region of the lunar south pole in 2018 [8].

There is also in course an amazing initiative called Google Lunar X Prize that consists in a total of $30 million in prizes to the first privately funded teams to safely land a robot on the surface of the Moon, have that robot travel 500 meters over the lunar surface, and send video, images and data back to the Earth.

The robotic space exploration looks promising in the next years to come but, despite its huge advantages, many scientist acknowledge that it alone is not sufficient and that humans are needed in space to perform more complex research tasks such as field geology or the acquisition and analysis of geological samples [9].

This is a strong incentive towards human spaceflight and, besides, there is also the natural impetus

for curiosity and adventure that the human being has shown in this kind of challenges that lead us to go further and further; not to mention the technological and industrial developments that always come associated to them. Nowdays, even the tourism industry has begun to recognize space as an interesting destination for the wealthy and some companies have already flown tourists to the ISS.

Human space exploration beyond LEO is presumably going to reemerge very soon specially if some of the present risks it poses are minimized.

Chapter 2

Radiation Environment in Space

"In principle, with enough money and expertise, it should be possible to build and fly a manned spacecraft to Mars and return safely to Earth. However, nobody knows yet how to deal with the dangerous cosmic radiation that floods through space." Oliver Angerer, ESA

Radiation is the term used for energetic particles or waves traveling in all directions through space or some medium. The particles or waves are produced or liberated by a source, and the source is said to radiate. Because radiation propagates through space and its energy is conserved in vacuum, the power of all types of radiation follows an inverse-square law of power with regard to distance from its source.

Before giving a more detailed description on radiation and the types of radiation that are of concern in a lunar mission it is necessary to stablish some basic concepts and quantities commonly used to describe radiation properties.

2.1 Basic Concepts

This section provides an overview of the basic physical concepts and definitions associated to radiation that will be used throughout the thesis. Most of the definitions come directly from physics and are purely mathematical but others arise from convention and are presented as defined by the International Commission on Radiological Protection (ICRP) and International Commission on Radiation Units and Measurements (ICRU). [10].

2.1.1 Fluence

Fluence, ψ, is the number of particles incident on a given area. It measures the particle areal density or the focus of a beam of partices. Fluence is expressed by the quotient of $\mathrm{d}N$ by $\mathrm{d}a$, where $\mathrm{d}N$ is the number of particles incident on a sphere of cross-sectional area $\mathrm{d}a$, thus

$$\psi = \frac{\mathrm{d}N}{\mathrm{d}a} \tag{2.1}$$

The IS unit of fluence is m^{-2}. The use of a sphere of cross-sectional area da expresses in the simplest manner the fact that one considers an area da perpendicular to the direction of each particle.

2.1.2 Fluence rate

Fluence rate, $\dot{\psi}$, the number of particles that pass through an area in a given time interval. It is the quocient of dψ by dt, where dψ is the increment of the fluence in the time interval dt, thus

$$\dot{\psi} = \frac{\mathrm{d}\psi}{\mathrm{d}t} \tag{2.2}$$

The IS unit of fluence rate is $m^{-2}s^{-1}$.

2.1.3 Flux

See fluence rate.

The term "flux" has been used historically by the nuclear community for fluence rate and also used for particle flux density, but its use has been discouraged by the ICRU convention to eliminate confusion between the terms "particle flux density" and "radiant flux"[11]. However the term "flux" is still common within the space weather and radiation protection communities for the quantity termed "fluence rate". Whenever the term "flux" appears in this thesis the units will be presented to avoid confusion (if by any means you find yourself confused just stick to the units shown).

2.1.4 Linear Energy Transfer

The linear energy transfer (LET) or restricted linear electronic stopping power, L_Δ, of a material, for charged particles of a given type and energy, is the quotient of dE_Δ by dl, where dE_Δ is the mean energy lost by the charged particles due to electronic interactions in traversing a distance dl, minus the mean sum of the kinetic energies in excess of Δ of all the electrons released by the charged particles.

$$L_\Delta = \frac{\mathrm{d}E_\Delta}{\mathrm{d}l} \tag{2.3}$$

The IS unit of LET is J m^{-1}; a frequently used unit is keV μm^{-1}.

2.1.5 Absorbed Dose

The absorbed dose is the measure of the amount of energy a body absorbed. The absorbed dose, D, is the quotient of d$\bar{E}$ by dm, where d$\bar{E}$ is the mean energy imparted by ionizing radiation to matter of mass dm, thus

$$D = \frac{\mathrm{d}\bar{E}}{\mathrm{d}m} \tag{2.4}$$

The IS unit of absorbed dose is J kg^{-1}. The special name for the unit of absorbed dose is gray (Gy);

1 Gy = 1 J kg^{-1}.

2.1.6 Dose equivalent

The dose equivalent, H, is the product of D and Q at a point in tissue, where D is the absorbed dose and Q the quality factor at that point. With D_L being the distribution of the dose D in LET L, and $Q(L)$ being the quality factor as a function of L in water we can write H as:

$$H = Q \times D = \int Q(L) D_L \, \mathrm{d}L \tag{2.5}$$

The IS unit of dose equivalent is J kg^{-1} with the special name sievert (Sv); 1 Sv = 1 J kg^{-1}.

The quality factor Q characterises the biological effectiveness of a radiation, based on the ionisation density along the tracks of charged particles in tissue. Q is defined by the ICRP as a function of the unrestricted linear energy transfer, L, of charged particles in water:

$$Q(L) = \begin{cases} 1 & L < 10 \quad \mathrm{keV}/\mu\mathrm{m} \\ 0.32L - 2.2 & 10 \leq L \leq 100 \quad \mathrm{keV}/\mu\mathrm{m} \\ 300/\sqrt{L} & L > 100 \quad \mathrm{keV}/\mu\mathrm{m} \end{cases} \tag{2.6}$$

Q has been superseded by the radiation weighting factor ω_R in the definition of equivalent dose (see section 2.1.7), but it is still used in calculating the operational dose equivalent quantities used in monitoring[12].

2.1.7 Equivalent dose

The equivalent dose, H_T, is the dose in a tissue or organ T given by:

$$H_T = \sum_R \omega_R D_{T,R} \tag{2.7}$$

where $\mathrm{D}_{T,R}$ is the mean absorbed dose from radiation R in tissue or organ T, and ω_R is the radiation weighting factor. This radiation weighting factor is dimensioneless and is used to reflect the higher biological effectiveness of high-LET radiations compared with low-LET radiations.

The IS unit for equivalent dose is the same as for the absorbed dose, J/kg, but with the special name Sievert (Sv).

The recommended numerical values for the ω_R of different radiations are given by ICRP [12] and are presented here in table 2.1. The weighting factor for neutrons (ω_n) is given as a function of the energy of the incident neutron (E_n) as can be seen in equation 2.8 and figure 2.1. For the other types of radiation the weighting factors are considered independent of the energy.

$$\omega_\mathrm{n} = \begin{cases} 2.5 + 18.2 e^{-(\ln E_\mathrm{n})^2/6}, & E_\mathrm{n} < 1\,\mathrm{MeV} \\ 5.0 + 17.0 e^{-(\ln 2E_\mathrm{n})^2/6}, & 1\,\mathrm{MeV} \leq E_\mathrm{n} \leq 50\,\mathrm{MeV} \\ 2.5 + 3.25 e^{-(\ln 0.04E_\mathrm{n})^2/6}, & E_\mathrm{n} > 50\,\mathrm{MeV} \end{cases} \tag{2.8}$$

Radiation Type	Radiation weighting factor, ω_R
Photons	1
Electrons, muons	1
Protons and charged pions	2
Alpha particles, fission fragments, heavy ions	20
Neutrons	A continuous function of neutron energy (see equation 2.8)

Table 2.1: Radiation weighting factors [12].

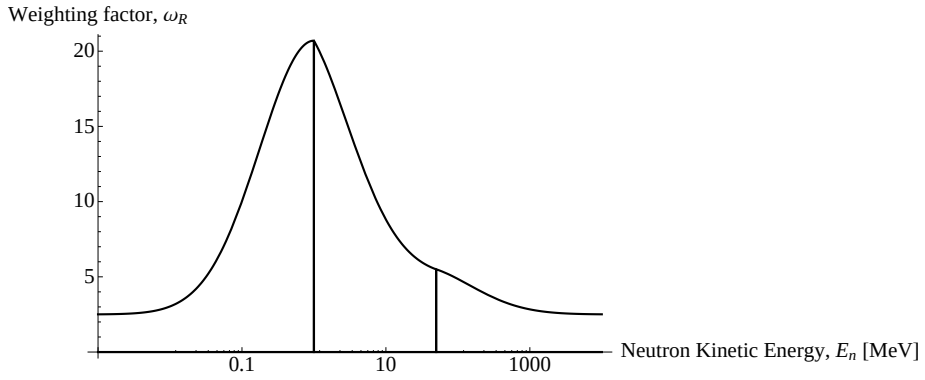

Figure 2.1: Radiation weighting factor for neutrons as a function of their kinetic energy when entering the tissue. The vertical lines are at 1MeV and 50MeV showing the boundaries of the function defined by parts in equation 2.8.

2.1.8 Ambient Dose Equivalent

The ambient dose equivalent, $H^*(d)$, at a point in a radiation field, is the dose equivalent that would be produced by the corresponding expanded and aligned field in the ICRU sphere (30 cm diameter soft-tissue-equivalent sphere with a density of 1 g cm^{-3} [13]) at a depth, d, on the radius vector opposing the direction of the aligned field. The IS unit of ambient dose equivalent is J kg^{-1} with the special name Sievert (Sv). For strongly penetrating radiation, a depth of 10 mm is recommended. The ambient dose equivalent for this depth is then denoted by $H^*(10)$.

2.1.9 Effective Dose

The effective dose, E, is the tissue-weighted sum of the equivalent doses in all specified tissues and organs of the body. It is defined as given in ICRP Publication 103 [12] by:

$$E = \sum_T \omega_T \sum_R \omega_R D_{T,R} \tag{2.9}$$

where ω_T is the tissue weighting factor with $\sum \omega_T = 1$. The sum is performed over all the organs and tissues of the human body listed ICRP publication 103 [12] and for all particles types R. The IS unit of effective dose is J/kg, with the special name Sievert (Sv).

The tissue weighting factor ω_T is used to represent the relative contribution of a specific tissue or organ to the total health detriment resulting from uniform irradiation of the body. It is weighted such

that $\sum_T \omega_T = 1$. The values for weighting factor of each organ accordingly to the ICRP recommendations are presented in table 2.2.

Tissue	**Tissue weighting factor, ω_T**	**Sum of ω_T values**
Bone-marrow (red), colon, lung, stomach, breast, remainder tissues[1]	0,12	0,72
Gonads	0,08	0,08
Bladder, oesophagus, liver, thyroid	0,04	0,16
Bone surface, brain, salivary glands, skin	0,01	0,04
Total	**-**	**1,00**

[1] Remainder tissues: Adrenals, extrathoracic region, gall bladder, heart, kidneys, lymphatic nodes, muscle, oral mucosa, pancreas, prostate (♂), small intestine, spleen, thymus, uterus/cervix (♀).

Table 2.2: Recommended tissue weighting factors given by ICRP [12].

2.1.10 Orbital Elements

To mathematically describe an orbit one must define six quantities, called orbital elements. They are: Semi-Major Axis; Eccentricity; Inclination, i; Argument of Periapsis, ω; Time of Periapsis Passage; Longitude of Ascending Node, Ω.

An orbiting satellite follows an oval shaped path known as an ellipse with the body being orbited, called the primary, located at one of two points called foci. An ellipse is defined to be a curve with the following property: for each point on an ellipse, the sum of its distances from two fixed points, called foci, is constant (see figure 2.2). The longest and shortest lines that can be drawn through the center of an ellipse are called the major axis and minor axis, respectively. The semi-major axis is one-half of the major axis and represents a satellite's mean distance from its primary. Eccentricity is the distance between the foci divided by the length of the major axis and is a number between zero and one. An eccentricity of zero corresponds to a circle [14].

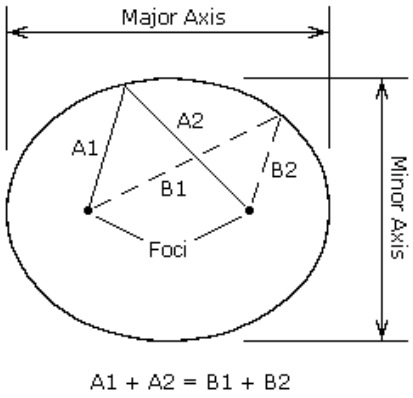

Figure 2.2: Ellipse curve [14].

Inclination is the angular distance between a satellite's orbital plane and the equator of its primary (or the ecliptic plane in the case of heliocentric, or sun centered, orbits), figure 2.3. An inclination of zero degrees indicates an orbit about the primary's equator in the same direction as the primary's

rotation, a direction called prograde (or direct). An inclination of 90 degrees indicates a polar orbit. An inclination of 180 degrees indicates a retrograde equatorial orbit. A retrograde orbit is one in which a satellite moves in a direction opposite to the rotation of its primary [14].

Periapsis is the point in an orbit closest to the primary. The opposite of periapsis, the farthest point in an orbit, is called apoapsis. Periapsis and apoapsis are usually modified to apply to the body being orbited, such as perihelion and aphelion for the Sun, perigee and apogee for Earth, perijove and apojove for Jupiter, perilune and apolune for the Moon, etc. The argument of periapsis is the angular distance between the ascending node and the point of periapsis (see Figure 2.3). The time of periapsis passage is the time in which a satellite moves through its point of periapsis [14].

Nodes are the points where an orbit crosses a plane, such as a satellite crossing the Earth's equatorial plane. If the satellite crosses the plane going from south to north, the node is the ascending node; if moving from north to south, it is the descending node. The longitude of the ascending node is the node's celestial longitude. Celestial longitude is analogous to longitude on Earth and is measured in degrees counter-clockwise from zero with zero longitude being in the direction of the vernal equinox. In general, three observations of an object in orbit are required to calculate the six orbital elements. Two other quantities often used to describe orbits are period and true anomaly. Period is the length of time required for a satellite to complete one orbit. True anomaly is the angular distance of a point in an orbit past the point of periapsis, measured in degrees [14].

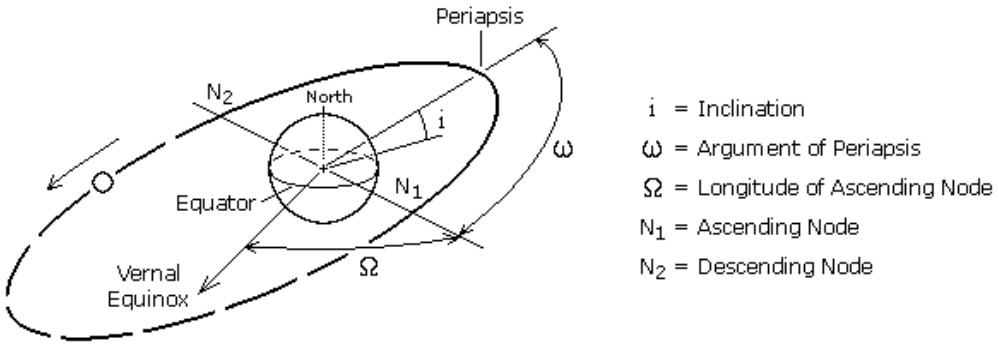

Figure 2.3: Orbital elements [14].

2.2 Types of radiation

2.2.1 Non-ionizing *vs* ionizing

Radiation can be roughly distinguished in two different types depending on how they interact with matter: ionizing radiation, if it has sufficient energy to ionize an atom; and non-ionizing radiation, otherwise. Ionization produced by particles is the process by which one or more electrons are liberated in collisions of the particles with atoms or molecules. The term ionizing radiation refers to charged particles (e.g., electrons or protons) and uncharged particles (e.g., photons or neutrons) that can produce ionizations in a medium or can initiate nuclear or elementary particle transformations that then result

in ionization or the production of ionizing radiation [11].

Near ultraviolet, visible light, infrared, microwave, radio waves and low frequency waves are common examples of non-ionizing radiation but of course this depends on the atoms that are present in the target that is being irradiated. Different atoms will have different ionization energies and in targets composed by a multitude of different elements this distinction between non-ionizing and ionizing radiation can be a bit fuzzy. The examples given before are the ones used when considering a target made of organic material. Organic tissue is essentialy made of carbon, hydrogen and oxygen, and the energies for the first ionization of atomic hydrogen and oxygen are both 13.6 eV [15]. Also, the energy of a single carbon-carbon bond is about 3.7 eV (it might vary a little depending upon what is attached to the two carbons). So, in radiobiology or when dealing with radiation protection in humans, it makes sense to choose an energy threshold around 10 eV above which the radiation is considered to be ionizing. According to the Planck-Einstein equation (equation 2.10), 10 eV correspond to a wavelength of 124 nm, which lies in the ultraviolet region of the electromagnetic spectrum, as can be seen in figure 2.4, therefore the boundary between non-ionizing and ionizing radiation is commonly considered to be in this region.

$$E = \frac{c}{\lambda} h \tag{2.10}$$

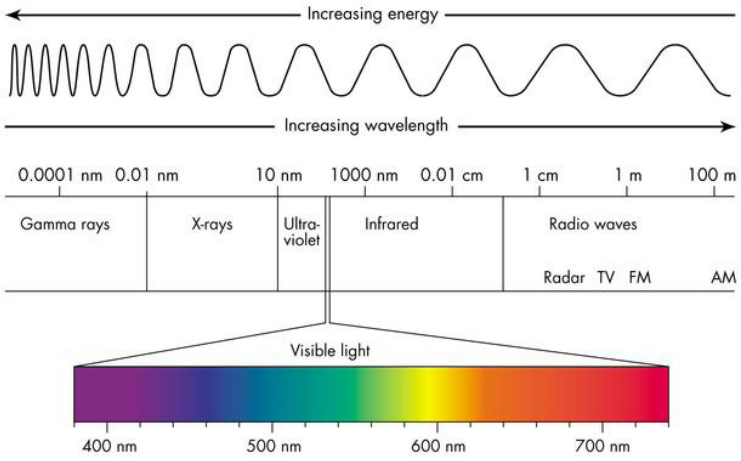

Figure 2.4: The electromagnetic espectrum.

Examples of ionizing radiation could be gamma rays, neutrons, alpha particles, beta particles, protons, electrons...

2.2.2 Cosmic Rays

In space a huge variety of radiations can be found from the cosmic microwave background to ultra high energy nuclei coming from still uncertain origins.

In the begining of the twentieth century Victor Hess detected that there was radiation penetrating the atmosphere from outer space. This discovery was later confirmed by Robert Millikan who gave the

radiation the name "cosmic rays". According to the ICRU, cosmic radiation is the ionizing radiation consisting of high-energy particles, primarily nuclei, of extra-terrestrial origin, and the particles they generate by interaction with the atmosphere and other matter [10].

In figure 2.5 are registered the fluence rates of all cosmic rays with respect to their energies. Notice that there are higher fluence rates of particles with energies up to around 100 GeV and that particles with much higher energies have very low fluence rates.

Figure 2.5 registers the fluence rates of all cosmic rays with respect to their energies. The cosmic rays spectre extends from a few MeV with high fluence rates up to around 100 GeV and may reach energies up to 10^{20} eV with fluence rates lower than 1 particle per km^2 during a year.

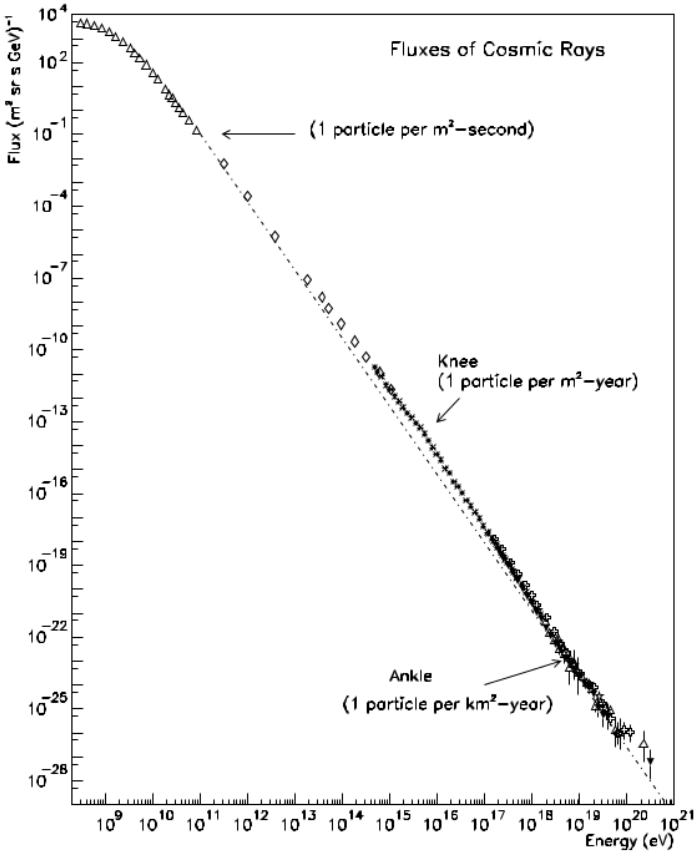

Figure 2.5: The all particle spectrum of cosmic rays [16].

2.2.3 Galactic Cosmic Radiation (GCR)

As the name suggests galactic cosmic rays are cosmic rays that have their origin within our galaxy but outside the solar system. Interplanetary space is bathed by a low fluence rate (particles per square meter per second or particles per square meter per steradian per second) of essentially uniformly distributed, highly energetic, and extremely penetrating ions that are believed to be accelerated by supernova shocks in our Galaxy [17]. These ions make up the GCR.

The highest-intensity GCR is found between a few tenths and a few tens of GeV per nucleon, where the particles can penetrate tens to hundreds of centimeters of shielding. Every naturally occurring

element in the periodic table is present in the GCR: nearly 90% are protons (hydrogen), close to 10% are helium, and the remaining percentage are elements heavier than helium, with a relative abundance roughly similar to that found in our solar system (figure 2.6).

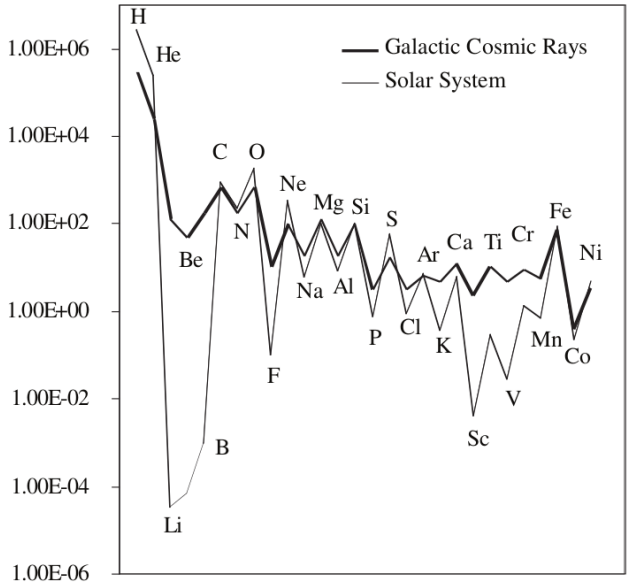

Figure 2.6: Relative abundance of elements in galactic cosmic rays and in the solar system. The very large GCR excesses at Li-Be-B and in the sub-Fe elements (Sc-Mn) are the products of spallation interactions during the cosmic rays' journey through the interstellar medium. SOURCE: Based on data from Astrophysics Science Division, NASA Goddard Space Flight Center Web site, available at `http://helios.gsfc.nasa.gov/ace/abund_plot.html`; `http://edmall.gsfc.nasa.gov/99invest.Site/ACEplot.html`. [18]

2.2.4 Solar Energetic Particles Event (SEP)

A solar particle event is an unusually large fluence rate of energetic protons, electrons and heavy ions ejected into space by a solar eruption. Solar particle events are directional. Despite having lower energy than the GCR the SEPs can be particularly dangerous for crews because of their high fluence rates.

The SEPs are in practice unpredictable but it was observed that they are more likely to occur during a solar maximum, often in the sequence of solar flares (SF) with coronal mass ejection (CME).

Solar maximum and solar minimum refer respectively to epochs of maximum and minimum sunspot counts in the sun. This epochs occur cyclically and correspond to higher or lower activity in the sun:

- The solar maximum is the time period of maximum solar activity during a solar cycle, usually defined in terms of maximum relative sunspot number or minimum GCR fluence rate. During this period SEPs are more likely to occur.
- The solar minimum is the time period of minimum solar activity during a solar cycle, usually defined in terms of minimum relative sunspot number or maximum GCR fluence rate.

The solar cycle has a period of approximately 11 years but cycles as short as 9 years and as long as 14 years have been observed. In figure 2.7 is shown a plot of the sunspot counts in the last ten solar cycles.

Figure 2.8 shows how sun activity cycles influence variations on the cosmic rays fluence rate.

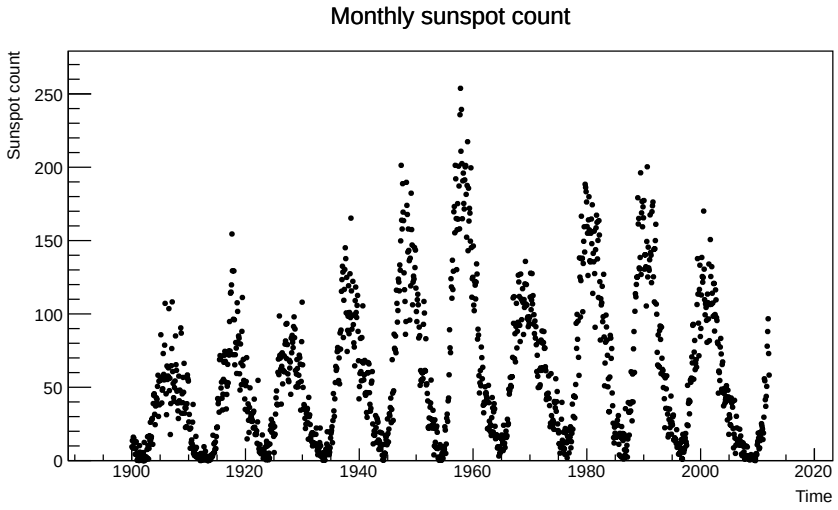

Figure 2.7: The monthly sunspot numbers for the latest 10 solar cycles.
(Data taken from `http://sidc.oma.be/sunspot-data/`)

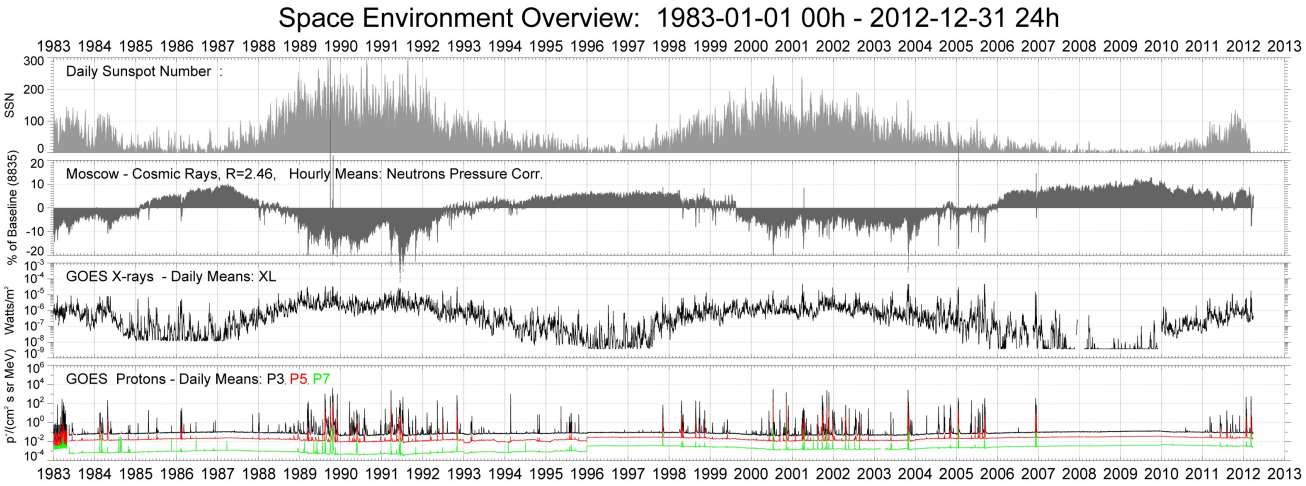

Figure 2.8: Five plots aligned in time showing (from top to bottom): sunspot counts, variation in neutron counting rate, X-ray energy flux (Watt/m^2) and protons fluence rate for energies from: 8.7 to 14.5 MeV (P3, black); 39.0 to 82.0 MeV (P5, red); and 110.0 to 500.0 MeV (P7, green).
(Data taken from `http://sxi.ngdc.noaa.gov`)

GCR fluence rate decreases during a solar maximum because the GCR particles lose energy in the more intense solar wind and are also more deflected by the sun magnetic field wich is stronger during that period.

2.2.5 Van Allen radiation belts (VAB)

The Van Allen radiation belts consist of energetic charged particles held in a torus around the Earth by the Earth magnetosphere. The belts were discovered in 1958 by a group of United States scientists under the direction of Dr. James Van Allen and named after him.

The Van Allen radiation is split into two distinct belts (figure 2.9), with energetic electrons forming

the outer belt, wich extends from roughly 15000 km to 25000 km altitude, and a combination of protons and electrons forming the inner belt, extending roughly from 1000 km to 6000 km altitude. Most of these protons and electrons come from solar wind thus the solar activity has a great influence on the amounts of radiation trapped in Earth magnetosphere.

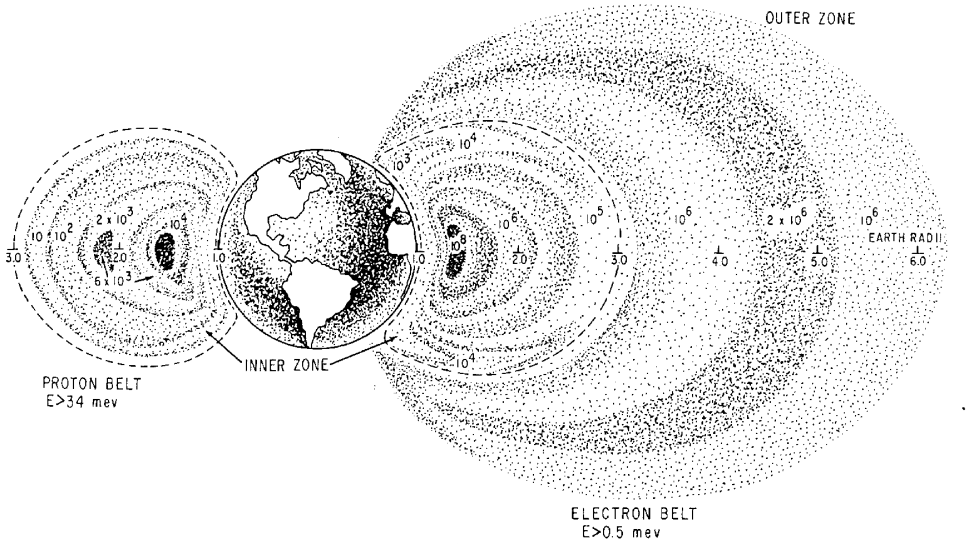

Figure 2.9: Ilustration of the Van Allen radiation belts evidencing the inner and outer belts. The greyed areas represent areas with approximately the same fluence rates (particles per square centimeter per second).

The motion of particles is strongly constrained by the local magnetic field. The basic mode is rotation around magnetic field lines, while at the same time sliding along those lines, giving the particles a spiral trajectory (see figure 2.10). The sliding motion slows down as the particle moves into regions where the magnetic field is strong, and it may even stop and reverse before the field line enters the atmosphere where the particle would lose energy possibly causing what is known as an aurora borealis or australis. Thus electrons and ions can remain trapped for a long time, bouncing back and forth from one hemisphere to the other. In addition to spiraling and bouncing, the trapped particles also slowly drift from one field line to another one like it, gradually going all the way around Earth. Ions for being positively charged drift one way (clockwise, viewed from north) and electrons the other way, and in either drift, the motion of electric charges is equivalent to an electric current circling the Earth clockwise.

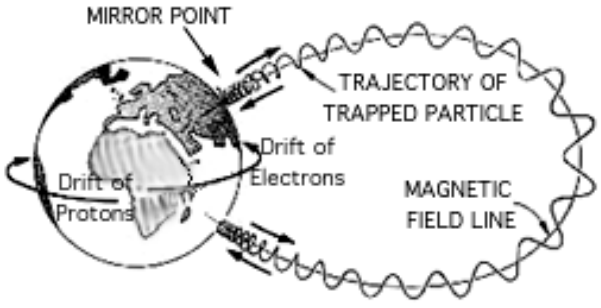

Figure 2.10: Motion of particles trapped in the radiation belts.

Earth is not a perfect dipole and its magnetic field presents some anomalies. Thus the radiation belts altitude vary over various parts of the Earth. The most significant case is over the south atlantic region, where the geomagnetic field draws particles closer to the earth. This region is known as the South Atlantic Anomaly (SAA) (figures 2.11 and 2.12).

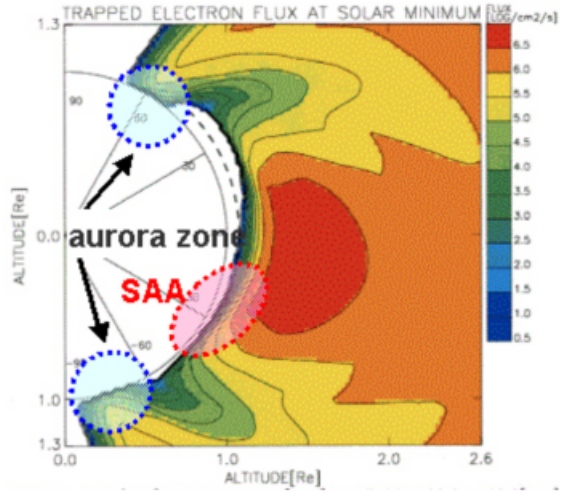

Figure 2.11: Map of fluence rate intensities for electrons in VAB evidencing the zones of aurora and SAA where the belts are closer to the Earth.

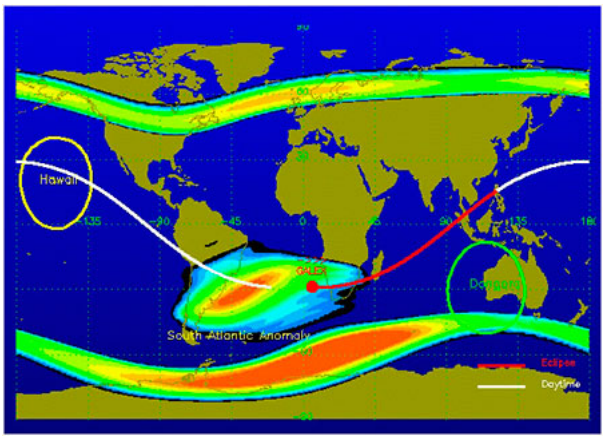

Figure 2.12: Map evidencing the regions where the VARB enter the atmosphere.

Radiation belts pose a hazard to satellites, which must protect their sensitive components with adequate shielding if their orbit spends significant time in the radiation belts. For crewed missions these radiation belts are also a significant threat, specially in missions beyond LEO. The timing and the path of the traversing of the radiation belts must be chosen carefully to meet periods of less activity in the sun, avoid the areas of greater fluence rates and reduce the time spent inside the belts.

As a curiosity, in the late 1950's and early 1960's, the radiation in Van Allen belts was temporarly intensified with an artificial belt of charged particles produced by the detonation of nuclear explosives being tested in space [19] [20]. The planets Jupiter and Saturn are also encircled by radiation belts similar to the Earth's Van Allen radiation belts.

2.2.6 Albedo

The albedo is the reflected radiation from a planet. Albedos can be for a specific wavelength or averaged over a range of wavelengths. The term is more commonly used for the reflected sunlight at visible wavelenghts (Bond albedo) but in this thesis it is essentially used to address the GCR reflected from the surface of the moon.

2.3 Lunar radiation environment

The moon is the natural satellite of our planet. It orbits the Earth at an average altitude of 384 400 km (semi-major axis) with a perigee of 362 570 km, an apogee of 405 410 km, an eccentricity of 0.0549 and an inclination between 18.29° and 28.58° to Earth's equator. The moon's orbital period is of 27,322

days. It has a mean radius of 1737 km. It's atmosphere is practically inexistent, a few elements produced by outgassing and sputtering have been detected but still the moon is considered to be surrounded by vacuum.

2.3.1 Lunar albedo

The moon is constantly being irradiated by solar wind and also GCR. Galactic cosmic rays that impact the lunar soil lose energy immediately through a series of intranuclear cascades. These cascades produce many secondary nucleons, mesons, and residual nuclei that will continue to lose energy through new cascades, decay and Coulomb collisions. Ultimately the residual particle population is dominated by neutrons with energies from fractions of eV's to about 100 MeV [21]. Figure 2.13 shows a measurement of neutron spectra acquired by the Lunar Prospector mission [21].

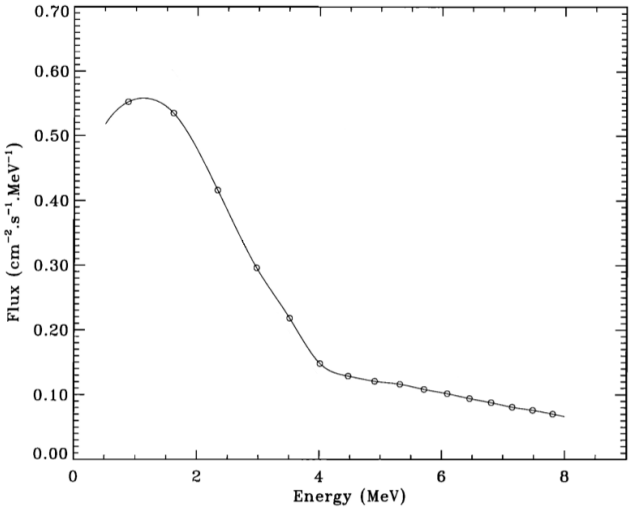

Figure 2.13: Flux spectrum of albedo neutrons from the moon and its cubic spline interpolation[21].

Albedo neutrons may be produced as deep as 1 meter into the soil and their flux is influenced by the soil composition. According to [22] these neutrons from lunar albedo contribute in less than 20% to the effective dose rate measured in the moon and its values are comparable to the uncertainty in the models for cosmic ray flux prediction. Despite this the albedo neutron fluxes are going to be included in the simulation model and the differences in resultant dose assessed.

2.3.2 Moon soil composition

When evaluating the albedo radiation from the surface of the moon, one must consider the lunar soil composition in order to make a reliable simulation because the nature of scattered radiation will depend strongly on the elements present in the lunar surface. For the calculation of the albedo at high altitudes we could consider an average composition of the lunar soil for the whole moon but as the altitude drops differences might arise depending whether we are above a lunar mare or a lunar highland. The composititon of the type of soil found in lunar mare and lunar highland is discriminated in table 2.3 as well as the average composition for the total surface of the moon. The data constant in table 2.3 was obtained mainly from samples colected during the Apollo missions [23].

Elements	**Mare** [%]	**Highland** [%]	**Average** [%]
O	60,3 ± 0,4	61,1 ± 0,9	60,9
Si	16,9 ± 1,0	16,3 ± 1,0	16,4
Al	6,5 ± 0,6	10,1 ± 0,9	9,4
Ca	4,7 ± 0,4	6,1 ± 0,6	5,8
Mg	5,1 ± 1,1	4,0 ± 0,8	4,2
Fe	4,4 ± 0,7	1,8 ± 0,3	2,3
Na	0,4 ± 0,1	0,4 ± 0,1	0,4
Ti	1,1 ± 0,6	0,2 ± 0,1	0,3

Table 2.3: Average chemical composition of lunar surface regolith in percentage of atoms [23].

The lunar soil is an important consideration in the development of an accurate model for the moon environment, however, in this work, a more straightforward approach was used. Given the availability of reliable measured data from probes such as the Lunar Prospector, real data was used for the lunar albedo instead of simulated one. In SRES the constitution of the lunar regolith is inserted for the porpuse of testing it as a shielding material.

Chapter 3

Biological Effects Of Radiation

"There are allowable limits for radiation going - I mean there's radiation all around us. There's radiation from your television set. There's radiation from your computer. There's radiation actually occurring in the ground." William Scranton

3.1 Radiation interactions in the human body

Space is a harsh environment. Nevertheless, engineering technology is capable of protecting astronauts against vacuum, extreme thermal conditions, and micrometeoroid environments. Protection from radiation, however, is much less straightforward. Before addressing the subject of radiation protection lets first understand how radiation exposure causes harm to the human body and what are the short and long term consequences.

In order to damage biological tissue radiation must interact physically with the tissue. These interactions occur at the atomic level and may turn out to be harmless or cause nocive effects that propagate to the failure of vital organs (figure 3.1).

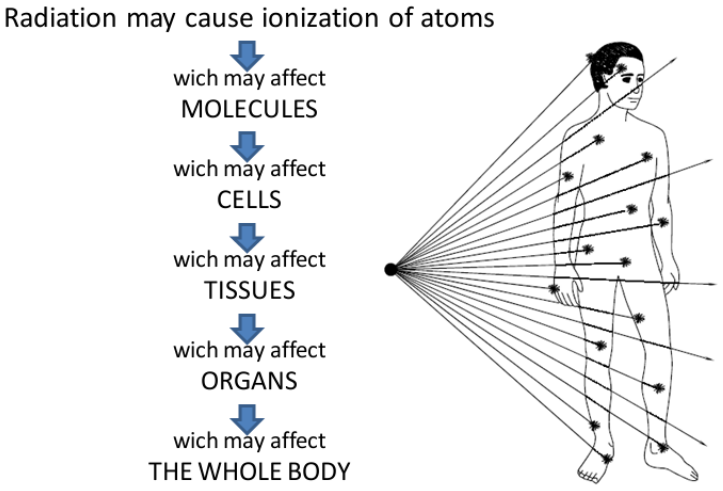

Figure 3.1: Diagram of the consequences caused by the propagation of the nocive effects from small scale to large scale in human body (adapted from [24]).

There are three ways galactic cosmic rays interact with matter:

- Ionization - figure 3.2(a) - One or more electrons are stripped from the atom. The atom becomes momentaneously charged and if it was binded to any molecule it may break away from that molecule causing it to lose it's functionality.
- Collision with nucleus - figure 3.2(b) - In the collision with a nucleus several secondary particles are generated and this may lead to an increased nocive effect. However the collision of the incident particle with a nucleus is a rare event given the fact that the nucleus only represents a small fraction of the size of the atom. It is far more likely that the interaction occurs with the electronic cloud than with the nucleus.
- Excitation - figure 3.2(c) - The incident particle excites an electron to an upper energy level within the atom. Usually no nocive effects come from this interaction as the charge in the atom is not changed and the electron promptly resumes to its initial energy level.

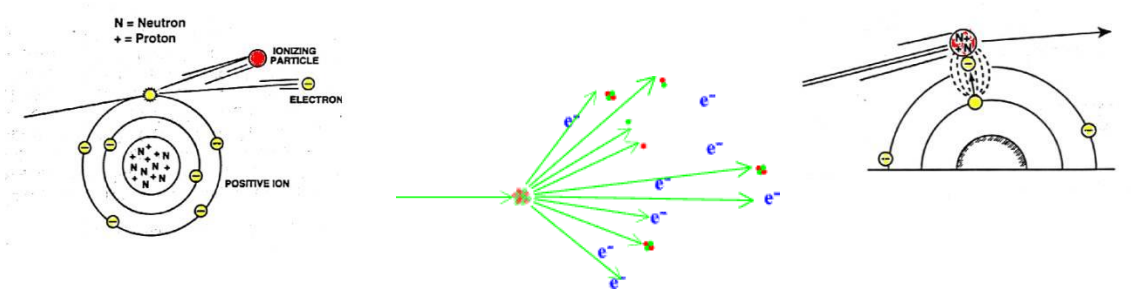

(a) Ionization (b) Collision with a nucleus (c) Excitation

Figure 3.2: Possible interactions of GCR with matter.

The ionization will be the most frequent type of interaction and also the one that raises greater concern given its capability to turn atoms into ions and possible break of chemical bounds.

3.2 Cellular damage

Even though all biological effects subsequent to radiation exposure can be traced back to the interaction of the radiation with atoms, there are two mechanisms by which radiation ultimately affects cells. These two mechanisms are commonly called direct and indirect effects [24].

The direct effects consist in radiation interacting directly with a DNA molecule or other cellular component critical to the survival of the cell (figure 3.3(a)). This interaction may affect the cells ability to reproduce and subsequently survive. If a sufficient amount of atoms in the DNA becomes affected in such a way that the cromossome cannot replicate itself or the information it contains is significantly changed then the cell suffers consequences that directly affect is chances of survival. The direct effects are predominant for radiation with higher LET such as neutrons, protons, alpha particles and heavier nucleus.

Indirect effects are the ones that occur when radiation changes a molecule or an atom in a way that it becomes a free radical roaming through the cell until it recombines with other cell component or functional structure creating compounds that might be toxical or sometimes inofensive. A good example of an indirect effect is the radiolytic decomposition of water (figure 3.3(b)). It consist in the separation of the water molecule into Hydrogen (H) and an hydroxyl group (OH) by the passage of an incident particle. This tow fragments may recombine themselves once againg forming water which is inofensive or form substances that are toxic to the cell and conntribute to its destruction such as hydrogen peroxide (H_2O_2).

Despite being relatively less dangerous to the cell the indirect effects occur more frequently than the direct ones, specially the radiolytic decomposition of water since water is highly abundant in the cellular medium. The direct effects are relatively less frequent since the nucleus represents just a fraction of the total volume of the cell but are extremely harmful to the cell and are at the origin of the majority of radiation diseases such as cancer.

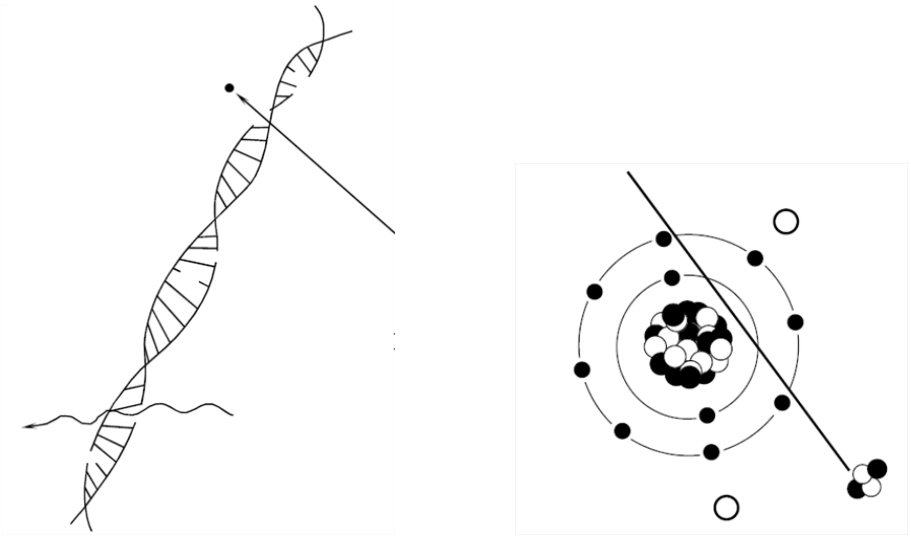

(a) Direct effect - Breaks in DNA sequence chains.

(b) Indirect effects - Radiolytic decomposition of water.

Figure 3.3: Types of effects responsible for damage of cellular structures (adapted from [24]).

When the DNA of a cell is damaged by radiation there are 4 possible outcomes for that cell (figure 3.4):

- The cell manages to completely repair the damage inflicted by the incident radiation and continues its functions normally.
- The cell dies due to the provoked damage.
- The cell manages to continue its vital functions but dies when it comes to replication.
- The cell is affected in a way that it does not die but suffers mutation. The mutated cell is still able to replicate and thus survive but the daughter cells are still mutations presenting non-repared damages and/or DNA aberrations.

The most undesired of this 4 scenarios is the last one. One might probably think that cellular death would be the worst case but as long as it does not occur to a large number of cells it is preferable than the survival of mutated cells since the body could expel the death cells and regenerate the tissue with healthy ones. Mutated cells are not expelled and are able to reproduce perpetuating the mutation and this could be the beginning of a malignant tumor.

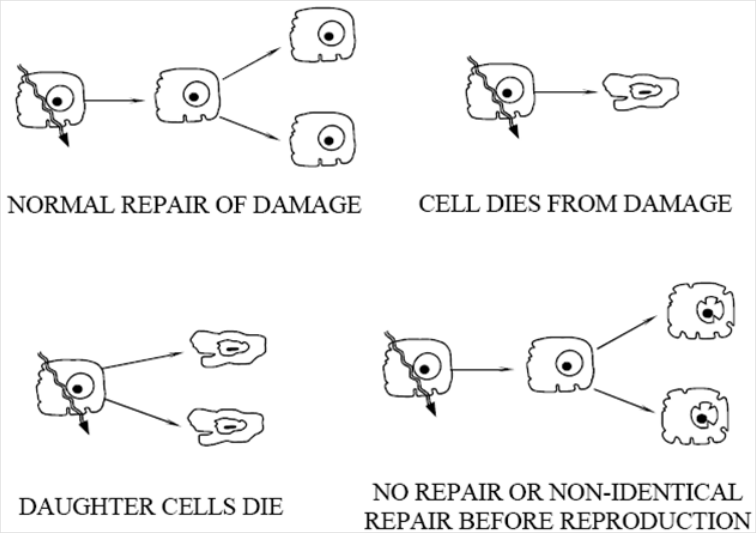

Figure 3.4: Possible outcomes for the evolution of an irradiated living cell [24].

3.3 Sensitivity to radiation and recommended dose limits

Not all tissues are equally sensitive to radiation. The sensitivity of the various organs of the human body correlate with the relative sensitivity of the cells from which they are composed. In general, tissues containing cells that are more actively regenerating are more sensitive to radiation. This is because cells that replicate more frequently have a greater need for its DNA information to be correct, and if the DNA is incorrect large amounts of cells with erroneous DNA would be reproduced causing the organ they belong to to fail earlier. The rate of reproduction of the cells forming an organ system is not the only criterion determining the overall sensitivity. The relative importance of the organ system to the well being of the body is also important. This measure of the overall sensitivity of an organ is expressed by the tissue weighting factor as seen in section 2.1.9. Therefore the organs that are more sensitive to radiation are (from the most sensitive to least sensitive):

-Blood forming organs;

-Gastrointestinal tract organs;

-Reproductive organs;

-Eyes;

-Skin;

-Muscles and brain.

Also the most common health issues associated to radiation include: cancer, cataracts, sterility, hair

loss, skin burns, nausea, fatigue, vomiting and diarrhea.

3.3.1 Recommended dose limits

Permissible exposure limits (PEL) for radiation exposure of astronauts have the primary functions of preventing in-flight risks that would jeopardize mission success and limiting chronic risks to acceptable levels based on legal, ethical or moral, and financial considerations. The European Space Agency uses limit values for the maximum dose in tissue largely based on the recommendations of the National Council for Radiological Protection (NCRP) for ground-based works with some modifications for 30-day and annual limits for non-cancer effects [25; 26]. The values of PEL used by ESA are presented in table 3.1 grouped by organ sensitivity and exposure interval - where they differ from the NCRP limits the NCRP limits are presented in parentheses.

Exposure Interval	**Equivalent Dose [Sv]**		
	Skin	Ocular Lens	BFO
30 Days	1.5	0.5 (1)	0.25
Annual	3	1 (2)	0.5
Career	6	4	1-4[1]

[1] Varies with gender and age at initial exposure, see table 3.2.

Table 3.1: Limits for equivalent dose in tissue.

Age at Exposure	Equivalent Dose [Sv]	
	Female	Male
25	1.0	1.5
35	1.75	2.5
45	2.5	3.2
55	3.0	4.0

Table 3.2: Career equivalent dose limits according to astronaut age and gender.

Crew members are not selected for missions if they are projected to exceed career limits at the end of any given mission. These limits are defined with the purpose of assessing the risk of exposure to radiation and are not to be interpreted as tolerance values. To ensure that astronauts do not approach radiation limits the"As Low As Reasonably Achievable" (ALARA) principle was set as a safety requirement for space missions. In short, the ALARA principle means making every reasonable effort to maintain exposures to ionizing radiation as far below the dose limits as practical.

Chapter 4

Lunar Mission Scenario Simulation

"Essentially, all models are wrong, but some are useful." George E. P. Box

The radiation exposure scenario in space missions can be very heterogeneous depending on whether the mission is within the magnetosphere (missions to the ISS for example) or in interplanetary space (as missions to the Moon and Mars). Here I will be considering the case of a crewed mission to the Moon. The mission will be divided in five phases and the environment for each phase will be simulated separately.

4.1 Lunar mission scenario

A mission to the moon comprises several stages. Figure 4.1 shows an example of the Apollo lunar missions profile. This example will be used as a reference for the lunar mission simulation in this work but the mission parts will be grouped in a different manner, considering a division in phases that are more adequate to the analysis of the radiation exposure. The division in phases was chosen according to five locations where the spacecraft passes, that present similar patterns of radiation environment. This way it becomes easier to simulate the conditions of the mission by focusing independently on each phase at a time.

The five mission phases chosen are here briefly described:

- LEO phase (200 to 2000 km altitude):
The LEO phase is the period during which the spacecraft is in the Low Earth Orbit zone (see table 4.1). This phase corresponds to step 6 in figure 4.1, it occurs just after Earth Orbit Insertion and before Trans Lunar Injection (TLI). This phase can last just a few minutes if the spacecraft is just passing through or a few days if rendezvous with already launched objects are scheduled. It is common to park spacecrafts in LEO for first checks after launch and to position the spacecraft in the desired trajectory. In the case of crewed missions to the moon the time spent in LEO is the minimum time needed to achieve a stable

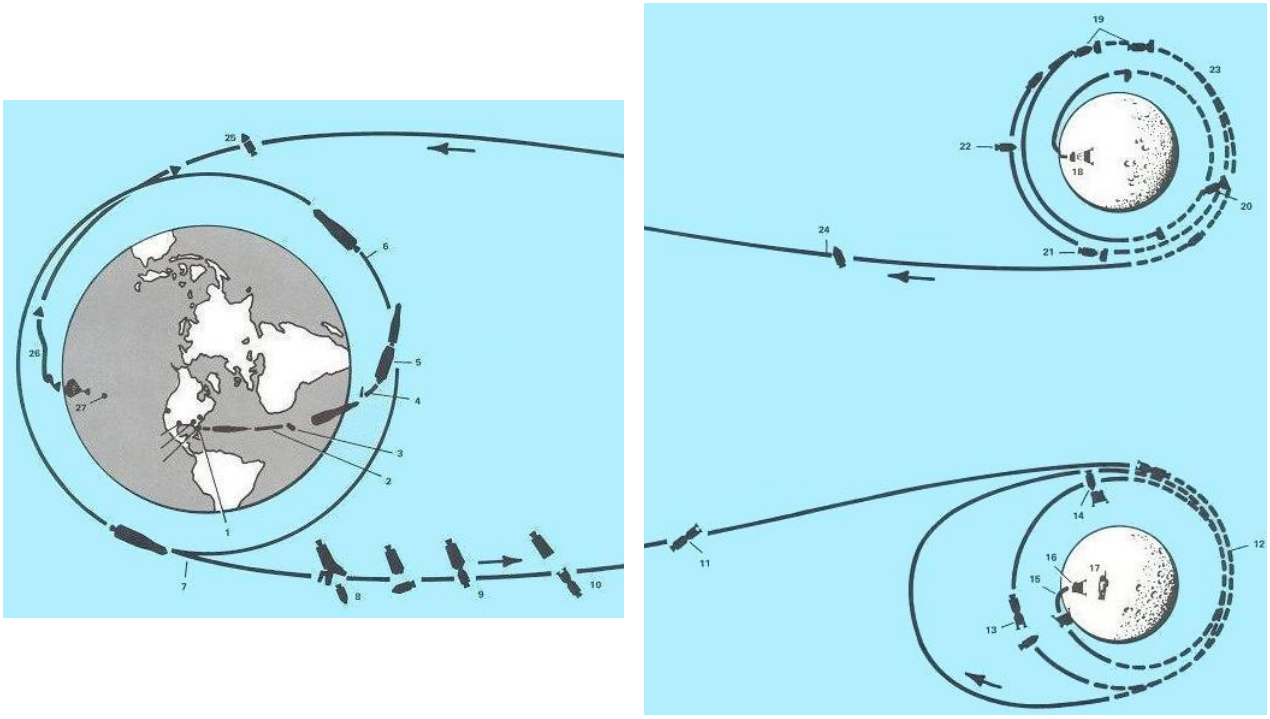

1 - Liftoff	10 - CSM/LM separation from S-IVB	19 - Rendezvous and docking
2 - S-IC powered flight	11 - Midcourse correction	20 - Transfer crew and experiment from LM to CSM
3 - S-IC/S-II separation	12 - Lunar orbit insertion	21 - CSM/LM separation and LM jettison
4 - Launch escape tower jettison	13 - Pilot transfer to LM	22 - Transearth injection preparation
5 - S-II/S-IVB separation	14 - CSM/LM separation	23 - Transearth injection
6 - Earth parking orbit	15 - LM descent	24 - Midcourse correction
7 - Translunar injection	16 - Touchdown	25 - CM/SM separation
8 - CSM separation from LM adapter	17 - Explore surface, set up experiments	26 - Communication blackout period
9 - CSM docking with LM/S-IVB	18 - Liftoff	27 - Splashdown

Figure 4.1: Mission profile of the Apollo expeditions to the Moon [27]. Dashed trajectory lines indicate loss of Earth comunications. The drawings are not to scale.

LEO orbit before the first window of opportunity to start TLI. The window of opportunity is when the spacecraft is traveling in the best portion of the Earth orbit that allows a TLI with minimum propellant consumption. This window of opportunity occurs once at each orbit revolution. In Apollo missions TLI was initiated after 1.5 revolutions (except for Apollo 17 that took 2 revolutions) which took about 2,5 to 3 hours depending on the altitudes where stable LEO was achieved [28]. In LEO phase the spacecraft benefits from the protection of the earth magnetic field but at some points of higher altitudes it is already influenced by the trapped radiation in the Van Allen Belts.

- Van Allen Belts (VAB) traversing phase (1000 to 25000 km altitude):

The VAB traversing phase occurs during the initial stage of the Translunar Injection, after the spacecraft leaves the LEO zone and before it enters the GEO (Geosynchronous Earth Orbit) zone. The inner belt is spread over altitudes from roughly 1000 to 6000 km and the outer one from 15000 to 25000 km. The Van Allen radiation belts are the most dangerous zone for the spacecraft, where the fluence rates are higher than in any other mission phases. The traversy of the Van Allen Belts is done choosing a trajectory that minimizes the time of passage through areas of higher fluence rates. In figure 4.2 is the

example of the translunar trajectory of Apollo 11, each dot in the trajectory of the Apollo 11 indicates its position after 10 min. The traversy took about 90 minutes and avoided the regions of maximum radiation intensity[29].

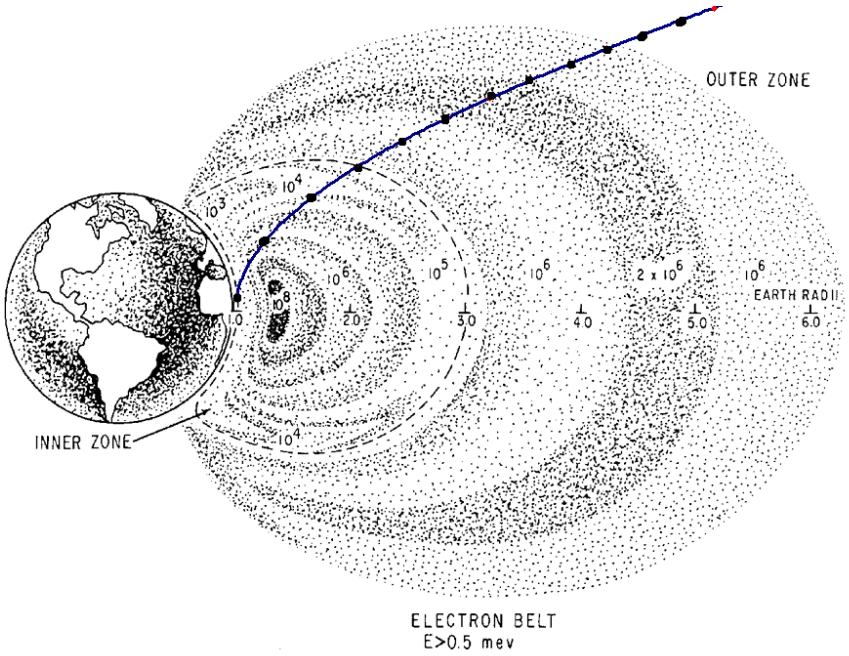

Figure 4.2: Apollo 11 trajectory through the Van Allen belts. The black dots indicate the time in 10 minute increments. [29]

- GEO phase or interplanetary phase (25000 to 380000 km altitude):

This is the phase where the spacecraft is at altitudes near the Geosynchronous Orbit. In this phase the spacecraft is already outside the influence of the Van Allen radiation belts thus no trapped particles are going to be considered here. The only sources of radiation considered here are GCR and SEP thus, in terms of radiation, this region is roughly equal to the rest of the interplanetary space except for the distance to the sun. In a mission to the moon this phase corresponds to the outbound just after leaving the Van Allen belts, this part of the trip is usually done in free flight, without propulsion, and it lasts about 3 days.

- Low Lunar Orbit (LLO) phase (100 km of altitude relative to the Moon):

This is the phase when the spacecraft enters lunar orbit. It is preceeded by the Lunar Orbit Insertion maneuver that is the sequence of burns to insert the spacecraft in its lunar parking orbit, usually LowLunar Orbit (LLO). Here the radiation sources considered are GCR, SEP and the lunar albedo neutrons.

- Surface Stay (SRF) phase (Moon surface):

The surface stay phase comprises all operation between moon landing and the ascent. The period of surface stay varies greatly deppending on mission purposes. Until now, the crewed missions of Apollo

program that landed on the Moon, spent from 22 hours to 3 days on the lunar surface, and 2 to 22 hours of extra vehicular activities (EVA) on the Moon [28]. The intent is to increase these periods and even to stay on the Lunar surface for an indefinite time, provided a shelter is built.

A summary of all mission phases is presented in table 4.1. SEP have to be taken into account as a radiation source for the scenario of a mission affected by a solar flare.

Mission phase	**Radiation types considered**	**Altitude [km]**	**Approximate duration**
LEO	GCR + trapped protons (+SEP)	200 – 2000	180 + 30 min
VAB traversing	GCR + trapped protons (+SEP)	1000 – 25000	90 + 90 min
GEO & Interplanetary	GCR (+SEP)	35786	3 + 3 days
Moon Orbit (LLO)	GCR + albedo neutrons (+SEP)	100	3 days
Moon Surface (SRF)	GCR + albedo neutrons(+SEP)	0	3 days

Table 4.1: Characteristics of each mission phase. The altitudes in Moon Orbit phase and Moon surface phase are relative to the Moon. The approximate duration depicts the approximate time spent in each phase considering as example the case of an astronaut onboard the Apollo 17 mission.

4.2 Simulation framework

Each of the five different mission phases will be simulated separately. The environment in each mission phase is basically characterised by the particle fluence rates that are obtained with CREME [30] for that particular region. CREME provides the particle fluence rates (in $[m^2\text{-s-sr-MeV/nuc}]^{-1}$) vs. the kinetic energy (in MeV/nuc) at the external surface of the spacecraft, before transport through shielding, given the orbit of the spacecraft and the environment conditions (sun activity and magnetosphere weather). After having the particle fluence rates in each phase, the transport and all subsequent calculations, such as deposited energy, doses and spectre of secondaries, is done using GEANT4 [31]. In figure 4.3 is a flowchart that elucidates how the different software modules are assembled and what are the inputs and outputs of the simulation.

For each mission phase three different weather scenarios were considered according to the sun activity. These scenarios are defined by CREME: Solar Minimum, Solar Maximum, and the worst case scenario of a Solar Flare. In the Solar Flare scenario the fluence rates correspond to the average of the intensity along 7.5 days, taking as a reference the solar flare that started on the 19^{th} October 1989, which is one of the most intense SEPs ever recorded. CREME also requires the spacecraft location, that can be inserted using the orbital parameters that define an orbit. For orbits inside the Earth's magnetosphere, the trapped proton model AP8max or AP8min, depending on the solar cycle conditions, must be chosen, as well as the geomagnetic weather conditions. Two magnetic weather levels are presently available in the CREME routine, a *quiet* magnetosphere (in which all fields are at nominal levels) and a very *stormy* magnetosphere (in which cosmic-ray access to Earth orbits is significantly increased). For calculations intended to reflect long-term averages, the quiet condition should be selected. However, for "worst case" and "peak rate" calculations, the *stormy* condition should be considered.

One must also decide the atomic species of the particles to insert for fluence calculation. The particle especies inserted were always from Z=1 to Z=28 considering the relative abundance of elements in GCR

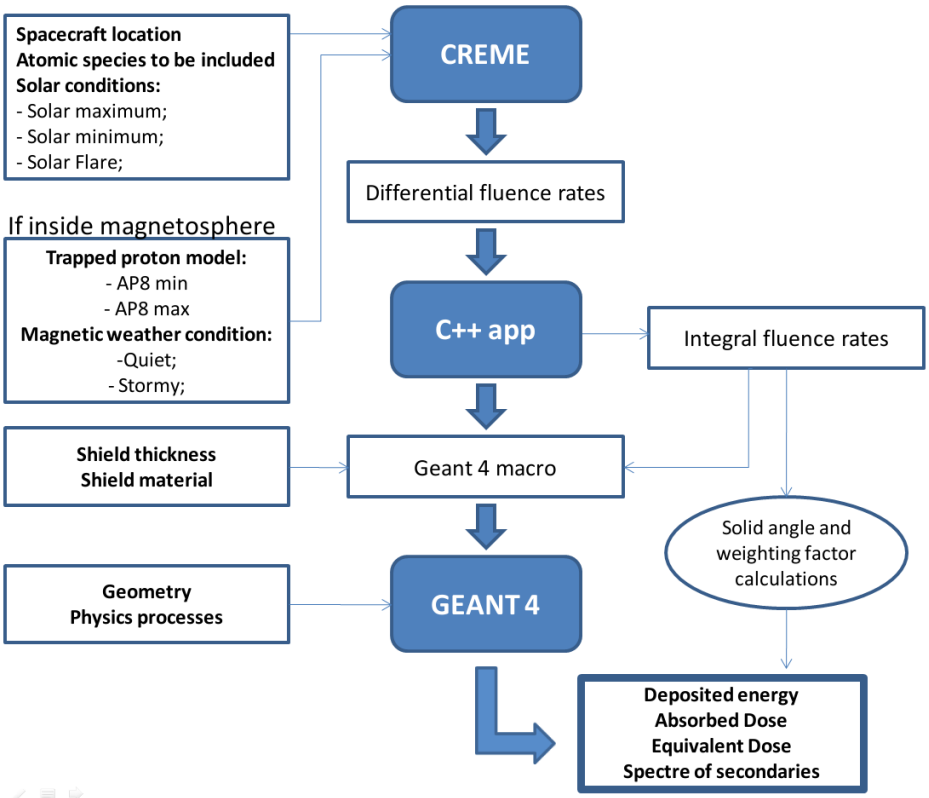

Figure 4.3: Flowchart evidencing the inputs on the left side and how the different software modules are integrated.

(2.6).

In order to compute the total fluence rates, the obtained differential fluence rates are then integrated. When integrating, it was taken into account that the width of the bins is not constant. In fact each bin is 1.0139 times larger than the previous one so that when plotted in a logarithmic scale every bin is equally spaced. More details on the integration method can be found in the appendix A.

A C++ script was written to automate the process of reading the differential fluence rate files, generate the integral fluence rate files and write the respective Geant4 macro.

4.2.1 CREME

CREME stands for "Cosmic Ray Effects on Micro-Electronics". It is a program suite developed by a team of scientists and engineers, led by the Cosmic Ray Physics Section of the High Energy Space Environment Branch at Naval Research Laboratory, that creates numerical models of the ionizing radiation environment in near-Earth orbits [30].

It is important to note that the environmental models used from CREME are subject to some limitations:

- The models are based on measurements near Earth. They can probably be used in orbits out to Mars (1.5 AU) but are not applicable to inner heliosphere or deep-space missions.

- Electrons, neutrons, and gamma-rays are not included in CREME models.

In general, when behind shielding, electrons and gamma rays do not contribute significantly to the dose comparing to protons and heavier ions. Neutrons are scarce in space [32] but they are present in lunar albedo and might be relevant when the spacecraft is near the moon (see section 2.3.1). For this reason, neutron fluence rates will be included using data from the Lunar Prospector [21].

The CREME software presents two GCR models: CREME96 and CREME2009. GCR dominate the spectrum at high energies (500-1000 MeV/nuc, depending upon element). CREME96 is a revision made in 1996 and is now based on data from 1950 to 1997. CREME2009 is a more recent version but does not support trapped protons yet, and so it will only be used for GEO phase. For the other phases (LEO and VAB) the CREME96 version was used.

4.2.2 GEANT4

Geant stands for "Geometry And Tracking", it is a C++ toolkit for the simulation of the passage of particles through matter, using Monte Carlo methods [31]. In Geant4 a generic geometry was built to test the effects of the exposure to radiation. The geometry is a simple sphere and the user has the option to set an spherical shielding shell around it with the desired thickness, ranging from 0 to 400 mm (figure 4.5). The materials used for the shield or sphere were created by giving the density of the material and its composition in percentage of elements. The list of materials defined and their compositions can be seen in figure 4.4. The material used for the sphere by default is the *TissueEquivalent* and the sphere radius is 15 cm, these values are chosen in order to reproduce the dimensions and constitution of the ICRU sphere used as a reference phantom in defining dose equivalent quantities [13]. The shielding material is by default an alluminium alloy widely used in aerospace industry for the construction of the spacecraft fuselage [33], its composition information was taken from [34].

TissueEquivalent	
Element Composition	**%**
H	10,10
C	11,10
N	2,60
O	76,20
Density [g/cm³]	1,00

Steel	
Element Composition	**%**
C	0,080
Fe	86,645
Cr	0,200
Ni	10,000
Mn	2,000
Si	1,000
P	0,045
S	0,030
Density [g/cm³]	8,03

Al2024_alloy	
Element Composition	**%**
Fe	0,50
Cr	0,10
Mn	0,50
Si	0,50
Cu	4,40
Mg	1,40
Zn	0,25
Ti	0,15
Al	92,20
Density [g/cm³]	2,78

LunarMareSoil	
Element Composition	**%**
O	60,30
Na	0,40
Fe	4,50
Si	17,00
Mg	5,30
Ti	1,20
Al	6,60
Ca	4,70
Density [g/cm³]	1,40

LunarHighlandSoil	
Element Composition	**%**
O	61,10
Na	0,40
Fe	1,80
Si	16,30
Mg	4,00
Ti	0,20
Al	10,10
Ca	6,10
Density [g/cm³]	1,40

LunarAverageSoil	
Element Composition	**%**
O	60,90
Na	0,40
Fe	0,30
Si	16,50
Mg	4,30
Ti	2,30
Al	9,50
Ca	5,80
Density [g/cm³]	1,40

Air	
Element Composition	**%**
N	70
O	30
Density [g/cm³]	1,29

Water	
Element Composition	**%**
H	66,70
O	33,30
Density [g/cm³]	1,00

LiquidHydrogen	
Element Composition	**%**
H	100
Density [g/cm³]	8,03

Vacuum	
Density [g/cm³]	1.e-25

Figure 4.4: Composition and density of the materials defined in Geant4 that can be directly used in the macro by the user.

In order to simulate the isotropic incidence of radiation all the geometry is placed inside a larger

spherical dome, with radius of 0.6 meters, from where the particles are fired inwards as can be seen in figure 4.6. The direction of the fired particles is uniformly distributed over a solid angle of 2π and the point from where they are fired is uniformly distributed over the inner surface of the dome.

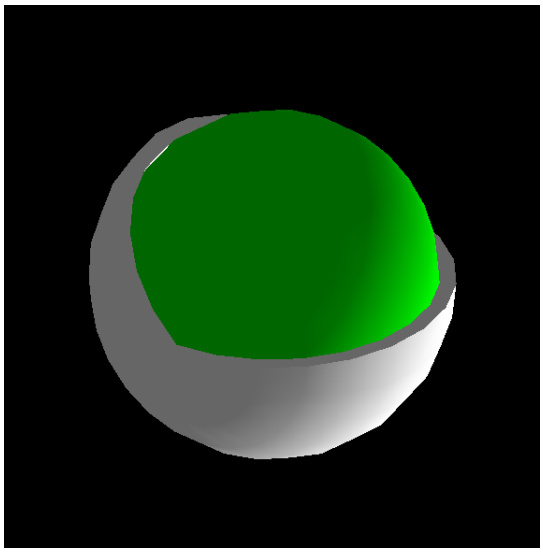

Figure 4.5: Geometry of the sphere with a cut in shield for better visualization. Different colours indicate volumes of different materials. (Image obtained from Geant4)

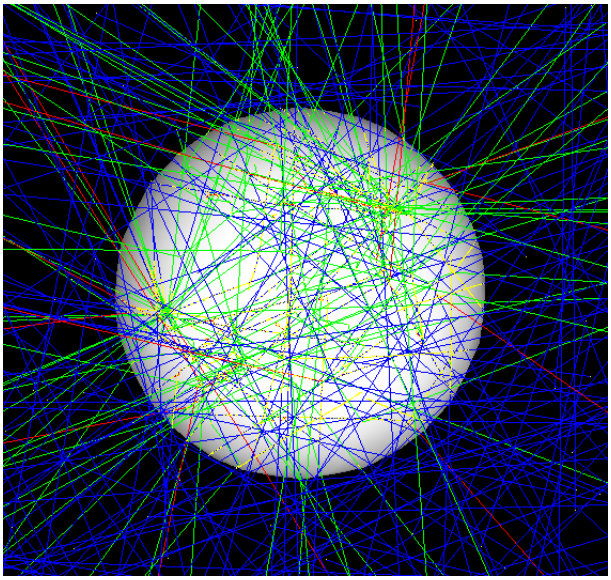

Figure 4.6: Sphere being irradiated. (Image obtained from Geant4)

The way the initial particles are fired into the geometry as well as their species, quantity and energies are defined externally through a macro that is read by the simulation just before the start of the Geant4 run.

Now one must not forget that the fluence rates given correspond to the ones felt at the external surface of the spacecraft and they come in units of particles per square meter per steradian per second. So, if we want to obtain the total number of particles per second that reach the environment inside the spherical dome in the simulation, we must multiply by the area of the spherical dome ($4\pi \times R^2$) and by the angular acceptance of each point in that area (2π). As an example, if the integration of the fluence rates in a given scenario is X $\mathrm{m^{-2}sr^{-1}s^{-1}}$, then, by multiplying by the area that is being irradiated and by the angular acceptance of that area, we get the total number of incident particles Y $\mathrm{s^{-1}}$. Given the spherical geometry used in this work the equation reads:

$$X\ [\mathrm{m^{-2}sr^{-1}s^{-1}}]\ \times\ 2\pi\ [\mathrm{sr}]\ \times\ 4\pi \times R^2\ [\mathrm{m^2}] = Y\ [\mathrm{s^{-1}}] \tag{4.1}$$

Y is the number of particles that actually should enter the dome but since the value used in the simulation is N_{gen}, in the end the results must be corrected by multiplying by the factor α:

$$\alpha = \frac{\text{Real number of particles}}{\text{Number of particles in simulation}} \Leftrightarrow \frac{Y}{N_{gen}} \tag{4.2}$$

Geant 4 has classes that contain different sets of physics processes to simulate the interaction of the particles with matter. In this work the classes used were "G4EmStandardPhysics" that contain

the electromagnetic processes and "HadronPhysicsQGSP_BERT" for the hadronic processes. For the case of lunar albedo "HadronPhysicsQGSP_BERT_HP", which includes a more accurate description of neutron interactions from thermal neutrons up to 200 MeV neutrons, was used.

The conditions for the calculation of the absorbed dose and equivalent dose were defined in the "MySensitiveDetector" class whitin the method "ProcessHits". The version of Geant4 used was the 9.4p02.

4.3 Implementation

The following sections give the details of the inputs used in each mission phase, present the differential and integral fluence rates, and the calculations of the solid angles and weighting factors when needed. The first results are also presented.

4.3.1 LEO phase

The orbit used to define the LEO conditions was chosen to be the ISS orbit because of its frequent use, this orbit is already precalculated in CREME so one does not need to set the orbital parameters. The trapped proton model used was the AP8MIN and AP8MAX for the solar minimum and solar maximum, respectively, and in both cases the magnetic weather was set as *quiet*.

The differential fluence rates obtained with CREME for solar minimum, solar maximum are soalr Flare conditions are shown in figures 4.7, 4.8 and 4.9, respectively.

The obtained integral fluence rates are presented in figures 4.10, 4.11 and 4.12.

4.3.2 Van Allen Radiation Belts (VAB) traversing phase

In order to obtain the CREME fluence rate tables we must set the trajectory through the VAB. This was done by choosing an orbit (in this case the orbit of the Apollo 11 mission during the Translunar injection was used) and then divide it in sections and ask for the fluence rates just for the desired sections. The following orbital elements (taken from [29]) were used for the highly elliptical orbit that contains the trajectory of the Apollo 11 during translunar injection:

- Apogee: 574 344 km;
- Perigee: 6 600 km;
- Inclination: 31.383°;
- Longitude of the ascending node: 358.380°;
- Displacement of the ascending node: 0°;
- Argument of perigee: 4.412°;

CREME offers the option to calculate the trapped protons for sections of the orbit delineated by the McIlwain L parameter [35] where L is in units of Earth radius (6371 km). The section corresponding

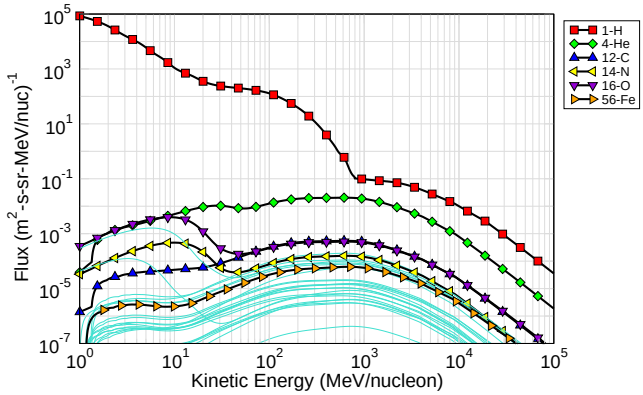

Figure 4.7: Differential fluence rate in LEO during Solar Minimum.

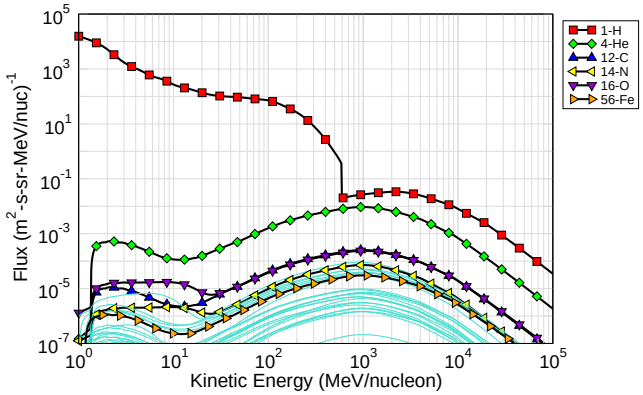

Figure 4.8: Differential fluence rate in LEO during Solar Maximum.

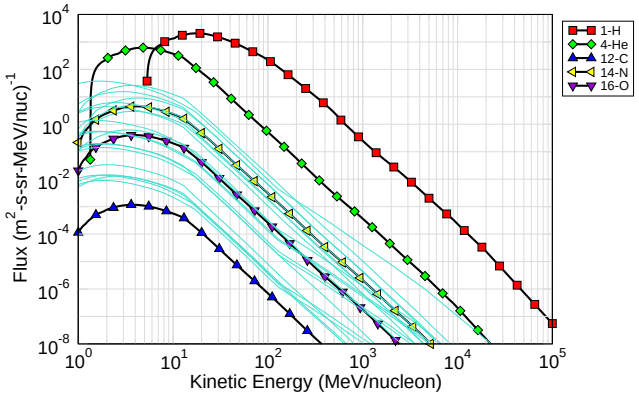

Figure 4.9: Differential fluence rate in LEO during Solar Flare.

to the VAB traversing phase was defined betwen L=1.3 and L=6. The fluence rates obtained for the trajectory that intersects the radiation belts are in the plots of figure 4.13, 4.14 and 4.15.

Using the same method as for the LEO phase the integral fluence rates were obtained and are displayed in figures 4.16, 4.17 and 4.18.

4.3.3 GEO phase or interplanetary phase

The differential fluence rates for GEO were obtained from CREME96 by especifying a GEO circular orbit, already precalculated in CREME, and are presented in figures 4.19, 4.20 and 4.21.

The integral fluence rates obtained are plotted in figures 4.22, 4.23 and 4.24.

4.3.4 Lunar Orbit phase

For the Lunar Orbit phase, the GCR (and SEP) were taken into account using the same fluence rates as for GEO phase, to which the fluence rates of the albedo neutrons were then added. The GCR (and SEP) and the albedo neutrons contributions were weighted according to the solid angle of the moon as seen by the spacecraft. Variations in the distance from the spacecraft to the moon change the solid

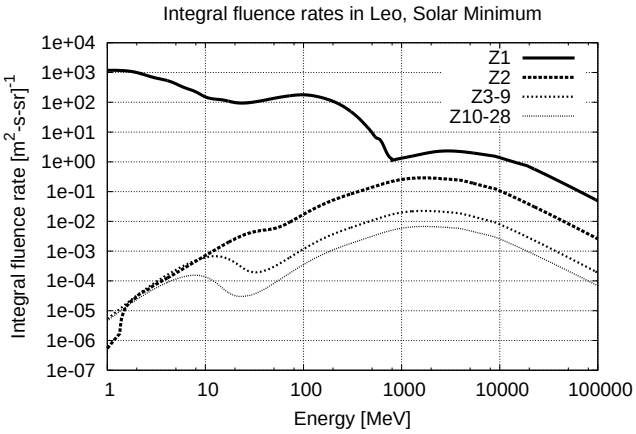

Figure 4.10: Integral fluence rate in LEO during Solar Minimum.

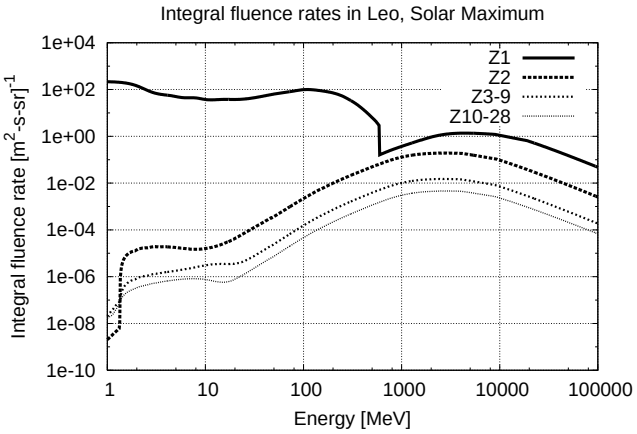

Figure 4.11: Integral fluence rate in LEO during Solar Maximum.

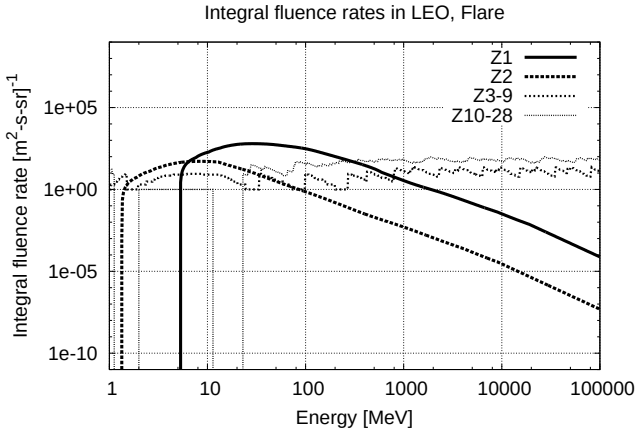

Figure 4.12: Integral fluence rate in LEO during Solar Flare.

angle. The solid angle Ω seen by the apex of a cone is calculated using the expression in equation 4.3 [36].

$$\Omega = 2\pi(1 - \cos\theta) \tag{4.3}$$

Where θ is half the angle of a cone with the apex located at the satelite and whose base fits the rim of the moon. Knowing the moon radius R_L, and considering that the spacecraft orbits at an average altitude of h, it is possible to obtain θ and thus get the solid angle as a function of the spacecraft altitude:

$$\sin\ \theta = \frac{R_L}{h + R_L} <=> \theta = \arcsin\left(\frac{R_L}{h + R_L}\right) \tag{4.4}$$

$$\Omega = 2\pi\left[1 - \cos\left(\arcsin\left(\frac{R_L}{h + R_L}\right)\right)\right] \tag{4.5}$$

The albedo neutrons were weighted by a factor $\frac{\Omega}{4\pi}$ and the GCR with the factor $\left(1 - \frac{\Omega}{4\pi}\right)$. So, for an

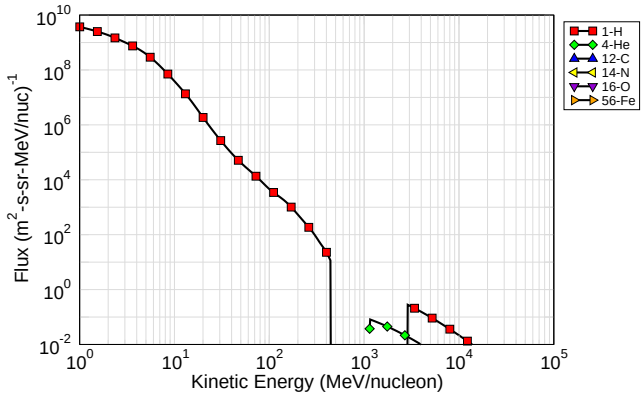

Figure 4.13: Differential fluence rate for the VAB traversing during a Solar Minimum.

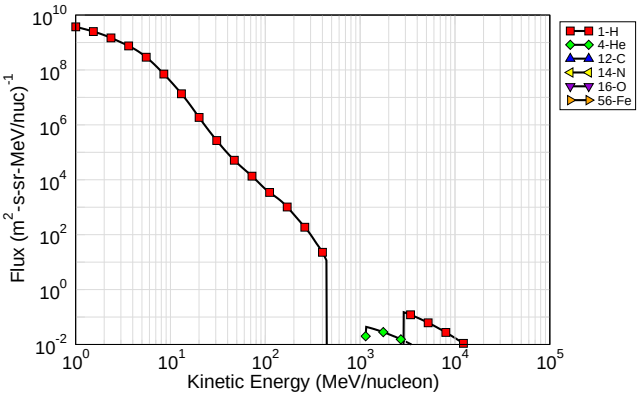

Figure 4.14: Differential fluence rate for the VAB traversing during a Solar Maximum.

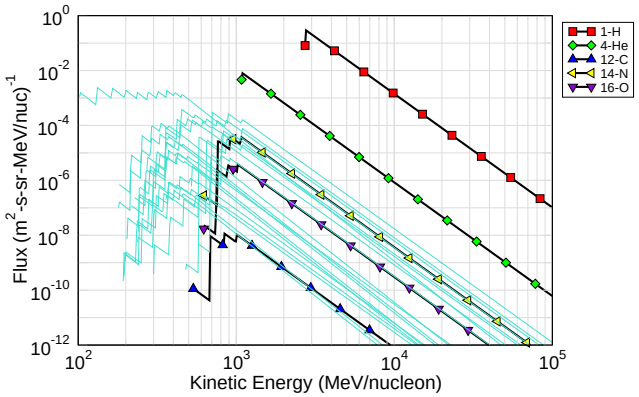

Figure 4.15: Differential fluence rate for the VAB traversing during a Solar Flare.

altitude of 100 km above the surface of the moon (in LLO) $\Omega = 4.24$ meaning that the moon occupies 33.7% of the sky seen by the spacecraft.

Lunar Prospector fluence rates (figure 2.13) are given in units of nuclei/cm^2-s-MeV. For dimensional consistence may be converted to nuclei/cm^2-s-sr. This convertion requires an integration in energy accounting to the variable bin width, and the satellite measuring acceptance for solid angle dependence.

The Lunar Prospector was able to measure the albedo neutrons coming from a 60x60 km area on the moon surface by orbiting at an altitude of 100 km and using a detector with a window of 150 cm^2. Comparing the area of the lunar surface scanned by the detector with the area of the window of the detector, we can consider the detector window to be point-like, as in the apex of a pyramid, the scanned area of the moon corresponding to the base of the pyramid (see figure 4.25).

The solid angle Ω seen by the apex of a rectangular pyramid, with base of side L and with high h, is given by equation 4.6 [36].

$$\Omega = 4\text{ArcTan}\left[\frac{L^2}{2h\sqrt{4h^2+2L^2}}\right] \tag{4.6}$$

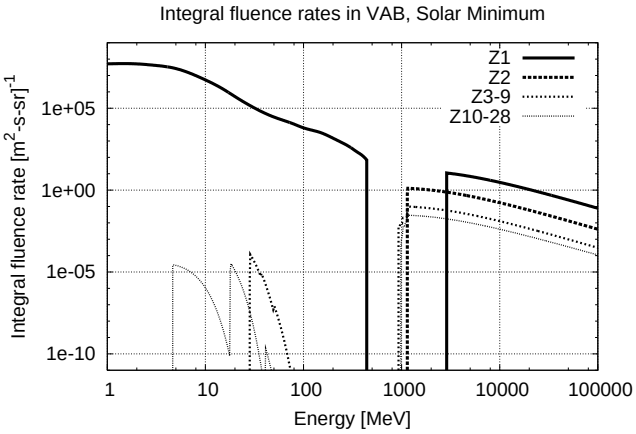

Figure 4.16: Integral fluence rate for the VAB traversing during a Solar Minimum.

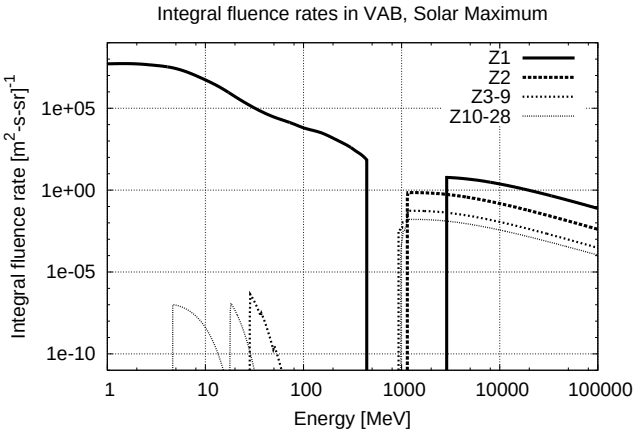

Figure 4.17: Integral fluence rate for the VAB traversing during a Solar Maximum.

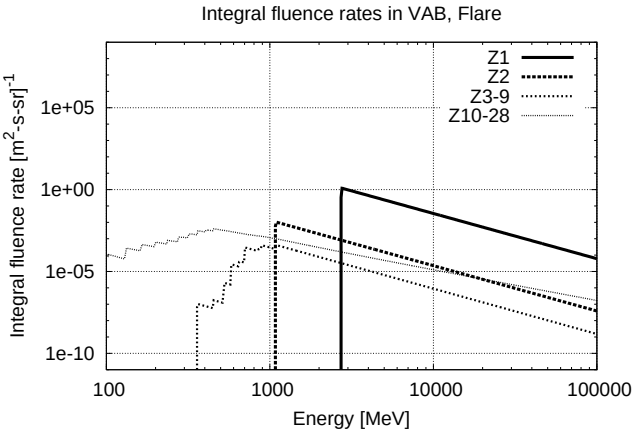

Figure 4.18: Integral fluence rate for the VAB traversing during a Solar Flare.

With L =60 km and h =100 km we obtain a solid angle Ω =0.3307 sr. Dividing the integral fluence rates by the solid angle and converting from cm^2 to m^2 we now get the integral fluence rates in the desired units, figure 4.26.

Albedo neutrons are generated by the interaction of GCR with lunar soil (section 2.3.1) so their fluence depends on GCR fluence. We have also seen that GCR fluence varies with the solar cycle (figure 2.8). The neutrons data was collected between 1998 and 1999 [5] during a solar minimum (figure 2.7). Therefore, Lunar Prospector data is here used to characterise the solar minimum scenario. For the solar maximum scenario the experimental neutron fluence rates were scaled down proportionaly to the GCR decrease. The scaling down factor was calculated by dividing the total intensity of GCR for the solar maximum by the total intensity for the solar minimum. The factor obtained was 0.4749.

The solar flare condition in Low Lunar Orbit is assumed to be similar to the GEO phase case.

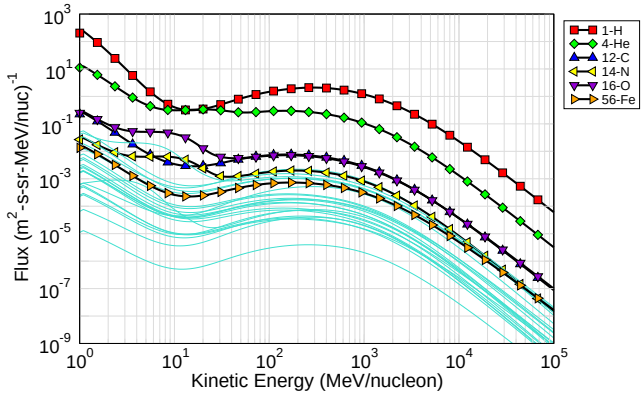

Figure 4.19: Differential fluence rate in GEO during Solar Minimum.

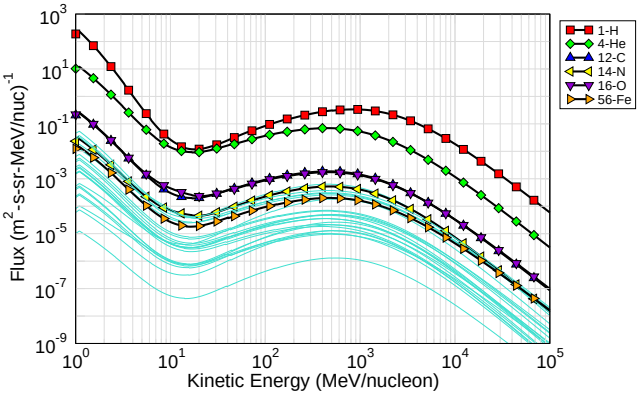

Figure 4.20: Differential fluence rate in GEO during Solar Maximum.

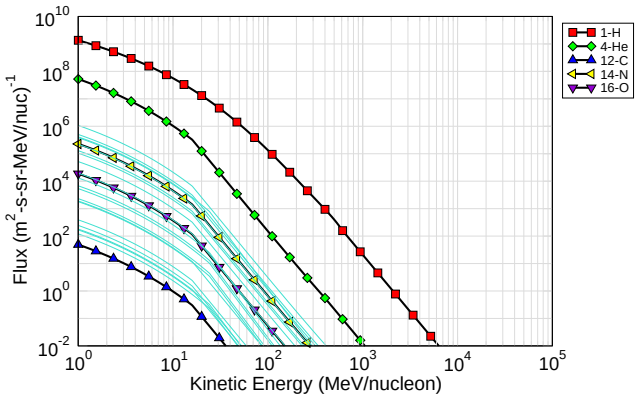

Figure 4.21: Differential fluence rate in GEO during Solar Flare.

4.3.5 Surface Stay phase

The way to simulate the radiation environment during the Lunar surface stay phase isn't much different from the lunar orbit phase. Here the only difference is that the solid angle of the moon will be 2π and the sky from where GCR (and SEP) come also has a solid angle of 2π, so the contributions of each type of radiation will be weighted by 0.5.

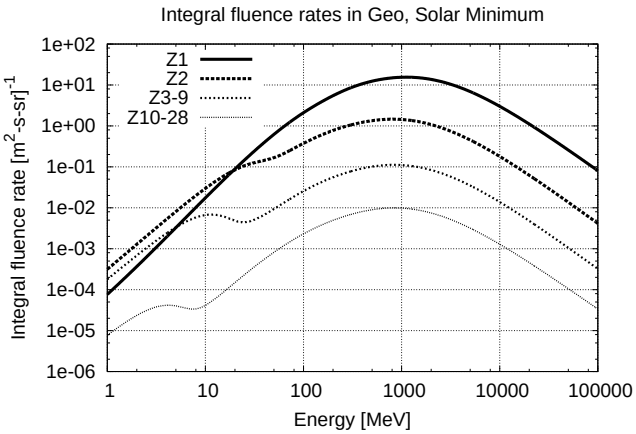

Figure 4.22: Integral fluence rate in GEO during Solar Maximum.

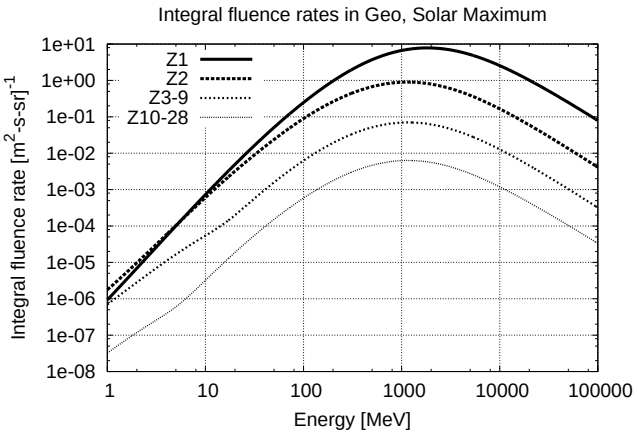

Figure 4.23: Integral fluence rate in GEO during Solar Maximum.

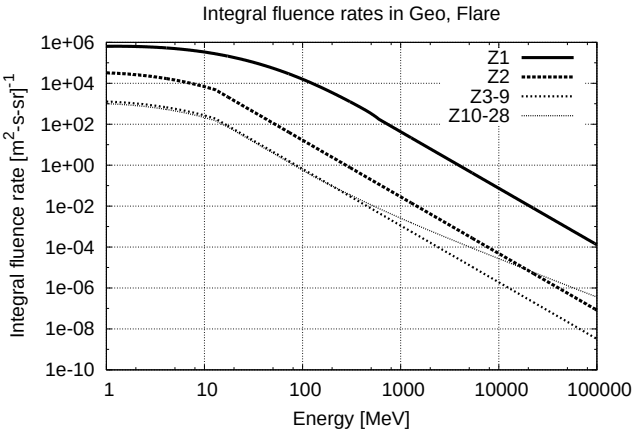

Figure 4.24: Integral fluence rate in GEO during Solar Flare.

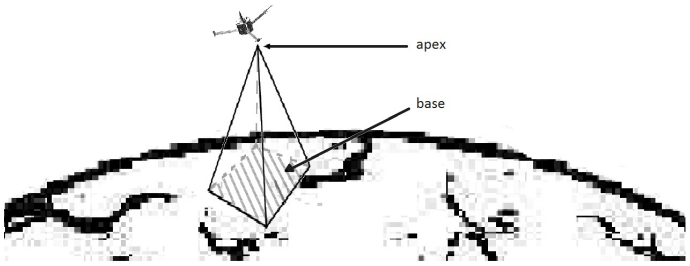

Figure 4.25: Representation of the solid angle aperture of the neutron detector in Lunar Prospector. (Not to scale.)

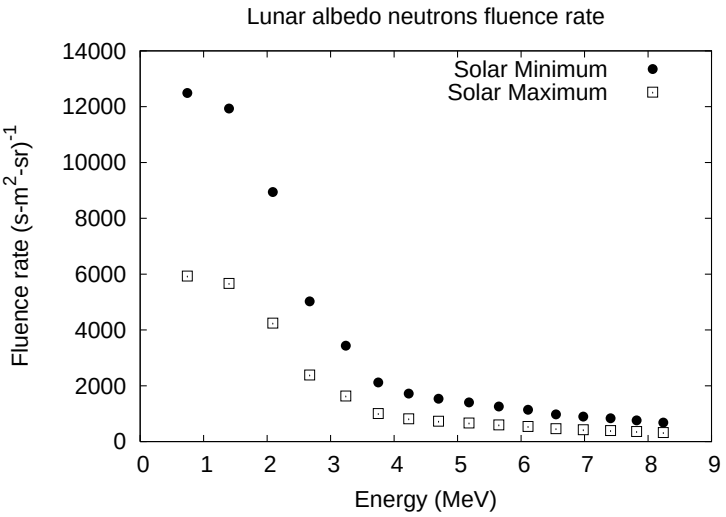

Figure 4.26: Integral fluence rate for lunar albedo neutrons.

Chapter 5

Results and Analysis

"Insanity: doing the same thing over and over again and expecting different results." Albert Einstein

This chapter gathers the results obtained with the methods described throughout sections 4.2 and 4.3. The different mission phases are compared as well as the effects of shielding.

5.1 Absorbed Dose

The results for absorbed dose, obtained with the SRES for each mission phase and weather scenario, are presented in table 5.1. The table also contains an estimate of the associated errors based on the statistics of each particle species contributing to the absorbed dose in the sensitive volume.

The data contained in the table is presented in figure 5.1 for the case with no shielding, and figure 5.2 shows the absorbed dose after an aluminium shielding shell with 10 cm thickness which corresponds to a shielding depth of 27,8 g/cm^2. This shielding depth lies whithin the typical values of shielding provided by the structural mass of crewed spacecrafts that might range from 10 to 40 g/cm^2 [37]. Looking at these figures one can imediatelly notice the high doses in VAB, due to the high fluence rates of particles trapped in the belts, and the differences of exposure to radiation from flares from zones inside the magnetosphere (LEO and VAB) to zones outside the magnetosphere (GEO, LLO and SRF). It is important to recall here that the Flare scenario is a transient event. The values presented in Flare are the variation felt in the environment if a SEP occurs. To evaluate the total dose during a SEP, the Flare value should be added to the respective *SolarMin* or *SolarMax* background value.

Comparing the two plots it is noticeable the high decrease in the absorbed doses resulting from flares in all mission phases when behind shielding. There is also a huge decrease of the dose coming from trapped protons in VAB. This is easily explained by the cut of the lower energy particles by the shield. Since the greater fluence rates come from protons (as can be seen in the integral fluence rate plots in section 4.3) it should be noted that the protons that surpasse a range of 27.8 g/cm^2 in aluminium must have kinetic energies above 180 MeV. A huge portion of the protons is being caught by the shield (see

Solar Conditions	Phase	Radiation type	Absorbed Dose [10^{-6} mGy/s]			
			No shielding	Err	27,8 g/cm^2	Err
Solar Minimum	LEO	Trap. protons	54,68	0,4%	6,45	3%
		GCR	1,80	3%	1,89	3%
	VAB	Trap. protons	3,755e+5	0,4%	59,3	6%
		GCR	3,03	3%	3,98	3%
	GEO	GCR	9,89	3%	9,88	3%
	LLO	Alb. neutrons	0,082	1%	0,179	2%
		GCR	6,55	3%	6,55	3%
	SRF	Alb. neutrons	0,118	1%	0,264	2%
		GCR	4,94	3%	4,94	3%
Solar Maximum	LEO	Trap. protons	28,03	0,4%	4,27	2%
		GCR	1,09	3%	1,33	3%
	VAB	Trap. protons	3,75e+5	2%	58,91	6%
		GCR	2,06	3%	2,71	3%
	GEO	GCR	5,34	3%	5,39	3%
	LLO	Alb. neutrons	0,015	1%	0,036	2%
		GCR	3,54	3%	3,57	3%
	SRF	Alb. neutrons	0,05	1%	0,122	2%
		GCR	2,67	3%	2,70	3%
Flare	LEO	SEP	97,94	0,4%	8,01	2%
	VAB	SEP	0,14	3%	0,212	3%
	GEO	SEP	1,901e+4	0,4%	193	2%
	LLO	SEP	1,260e+4	0,4%	128	2%
	SRF	SEP	9504	0,4%	96,4	2%

Table 5.1: Absorbed dose values obtained for all considered scenarios.

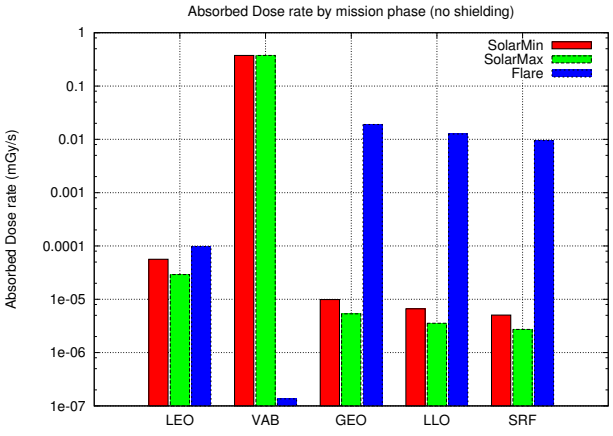

Figure 5.1: Absorbed dose rates for each weather scenario by mission phase (SRF represents the lunar surface phase). No shielding was considered.

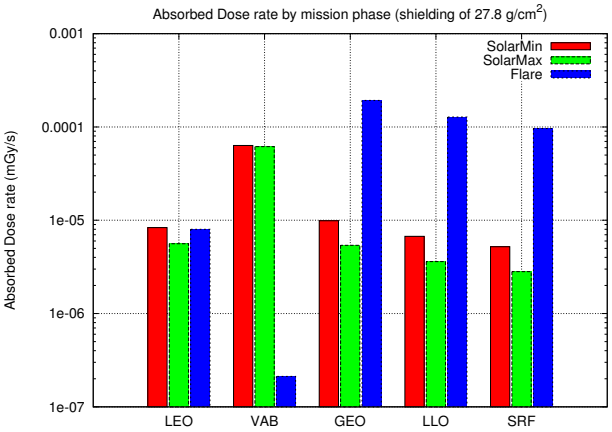

Figure 5.2: Absorbed dose rates after a shield of 27,8 g/cm^2 of Aluminium (100mm).

fluence rate espectres below 200 MeV in figures 4.16 and 4.17). On the other hand, the dose for *SolarMin* and *SolarMax* scenarios in GEO, LLO and SRF, barely changes because in this phases the dominant particle radiation consists mainly of high energy GCR that can easily pass through the shielding.

The values obtained with SRES for absorbed doses are consistent with already published works on space radiation. Doses, without shielding, of 0.9 mGy per day (1.04×10^{-5} mGy/s) are mentioned for the Skylab (435 km altitude) [38] and biodosimetry studies of astronauts who have stayed in the ISS (shielded by the space station) revealed doses of 85 mGy per 6 month (5×10^{-6} mGy/s) [39]. The results obtained for VAB and GEO are also concordant with other works [40].

Solar Conditions	Phase	Radiation type	Equivalent Dose [10^{-6} mSv/s]			
			No shielding	Err	27,8 g/cm^2	Err
Solar Minimum	LEO	Trap. protons	109,4	0,4%	16,6	3%
		GCR	17,8	3%	20,6	2%
	VAB	Trap. protons	7,510e+5	0,4%	220	6%
		GCR	32,1	3%	40,1	2%
	GEO	GCR	81,2	3%	62,1	3%
	LLO	Alb. neutrons	3,32	1%	1,95	1%
		GCR	53,82	3%	41,2	3%
	SRF	Alb. neutrons	4,80	1%	3,16	1%
		GCR	40,61	3%	31,1	3%
Solar Maximum	LEO	Trap. protons	56,05	0,4%	12,6	2%
		GCR	11,55	3%	23,7	2%
	VAB	Trap. protons	7,50e+5	2%	202,8	6%
		GCR	22,7	3%	26,7	2%
	GEO	GCR	50,1	3%	44,8	2%
	LLO	Alb. neutrons	0,59	1%	0,41	2%
		GCR	33,2	3%	29,7	2%
	SRF	Alb. neutrons	2,15	1%	1,29	2%
		GCR	25,0	3%	22,4	2%
Flare	LEO	SEP	227,2	0,4%	22,1	2%
	VAB	SEP	0,53	3%	1,17	2%
	GEO	SEP	4,263e+4	0,4%	631	1%
	LLO	SEP	2,825e+4	0,4%	418	1%
	SRF	SEP	2,131e+4	0,4%	315	1%

Table 5.2: Equivalent dose values obtained for all considered scenarios.

5.2 Equivalent Dose

The equivalent dose rates in figures 5.3 and 5.4 present similar characteristics to the absorbed dose rates. The equivalent dose accounts for the biological sensitiveness to radiation depending on its particle composition as seen in section 2.1.7. Since the espectre of incident particles is mainly dominated by protons in each phase, the equivalent dose plot for no shielding appears almost just as an increment of the absorbed dose plot. However, when behind shielding secondary particles are generated wich have different weighting factors and the differences between the two quantities become more evident.

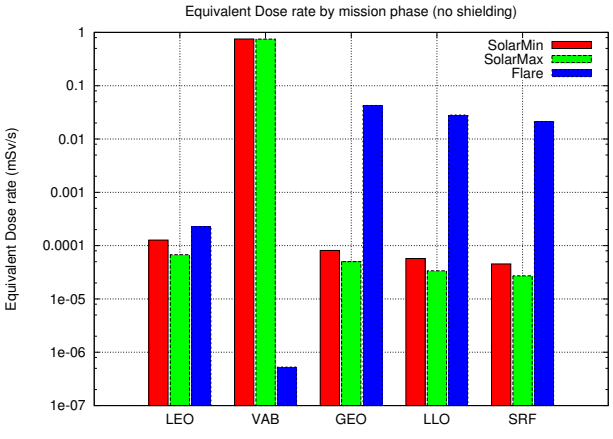

Figure 5.3: Equivalent dose rates for each weather scenario by mission phase. No shielding was considered.

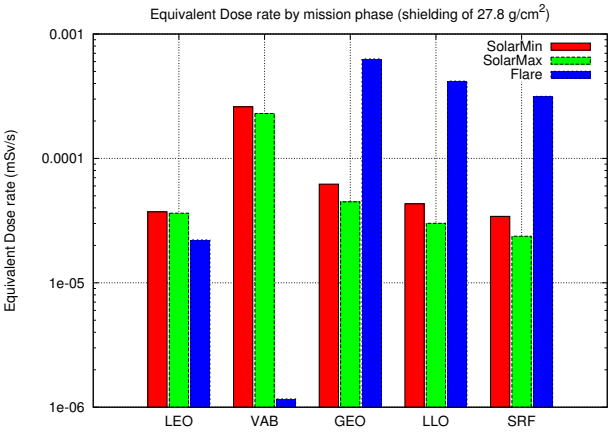

Figure 5.4: Equivalent dose rates after a shield of 27,8 g/cm^2 of Aluminium (100mm).

As expected, the Van Allen Belts is the most risky area, even when behind shielding, but it is also

the phase where less mission time is usually spent.

5.3 Lunar Mission Scenarios

By multiplying the equivalent doses in each phase by the time the mission is expected to spend in that phase, we get the total dose for the mission. These doses should now be compared with the PEL for astronauts in order to estimate the risk of radiation exposure. We have seen in section 3.3.1 that blood forming organs (BFO) are the most sensitive to radiation with permissible exposure limits of 0,25 Sv for 30 days exposure and 0.5 Sv for annual exposure. Tables 5.3, 5.4 and 5.5 show the doses already integrated for the lunar mission time and contain below the totals. Being correct, these are the values that a dosimeter would supposedly register if it accompanied the astronauts during the trip to the moon. The time for each mission phase was based on the Apollo 17 mission: 210 minutes in LEO, 180 minutes in VAB, 6 days in GEO, 3 days in LLO and 3 days at SRF. Figure 5.5 shows the equivalent doses for each mission phase integrated in these times (bars) and the sum of the equivalent doses in all phases, for solar minimum and solar maximum scenarios (the two lower horizontal lines), also the dose limits, recommended by ESA, for 30 day and annual exposure in BFO are shown (the two upper horizontal lines). In LEO and VAB phases the equivalent doses are lower than in the other phases, essentially because it is where less time is spent, but also because of the protection of the magnetosphere which cuts a huge part of the particles that come from flares which have the highest contribution to dose in phases outside the magnetic field of the earth.

Mission Phase		Absorbed Dose [mGy] (27,8 g/cm^2)	Equivalent Dose [mSv] (27,8 g/cm^2)
Solar Minimum	LEO	0,11	0,47
	VAB	0,68	2,81
	GEO	5,12	32,21
	LLO	1,74	11,18
	SRF	1,35	8,87
	TOTAL	**9,00**	**55,53**

Table 5.3: Total absorbed and equivalent doses for a lunar mission during a period of solar minimum.

Mission Phase		Absorbed Dose [mGy] (27,8 g/cm^2)	Equivalent Dose [mSv] (27,8 g/cm^2)
Solar Maximum	LEO	0,07	0,46
	VAB	0,67	2,48
	GEO	2,79	23,23
	LLO	0,94	7,80
	SRF	0,73	6,14
	TOTAL	**5,20**	**40,11**

Table 5.4: Total absorbed and equivalent doses for a lunar mission during a period of solar maximum.

Notice that a single flare event when in GEO, LLO or in the Moon surface (outside the Earth magnetosphere) may exposure the crew to more dose than the total of the mission without any flare, this could be fatal. Remember that the flare doses presented here are from the October 1989 which is one of the most intense SEPs and, in this example, it even reaches the 30 day dose limit. Flares present a serious threat to missions outside the magnetosphere and as space missions tend to last longer it is possible that more than one large flare occurs during a mission.

Mission Phase		Absorbed Dose [mGy] (27,8 g/cm^2)	Equivalent Dose [mSv] (27,8 g/cm^2)
Flare	LEO	0,10	0,28
	VAB	0,002	0,013
	GEO	100,0	326,9
	LLO	33,1	108,3
	SRF	25,0	81,7
	TOTAL	**158,19**	**517,21**

Table 5.5: Total increment in solar minimum or solar maximum doses if a large solar flare occurs during a lunar mission.

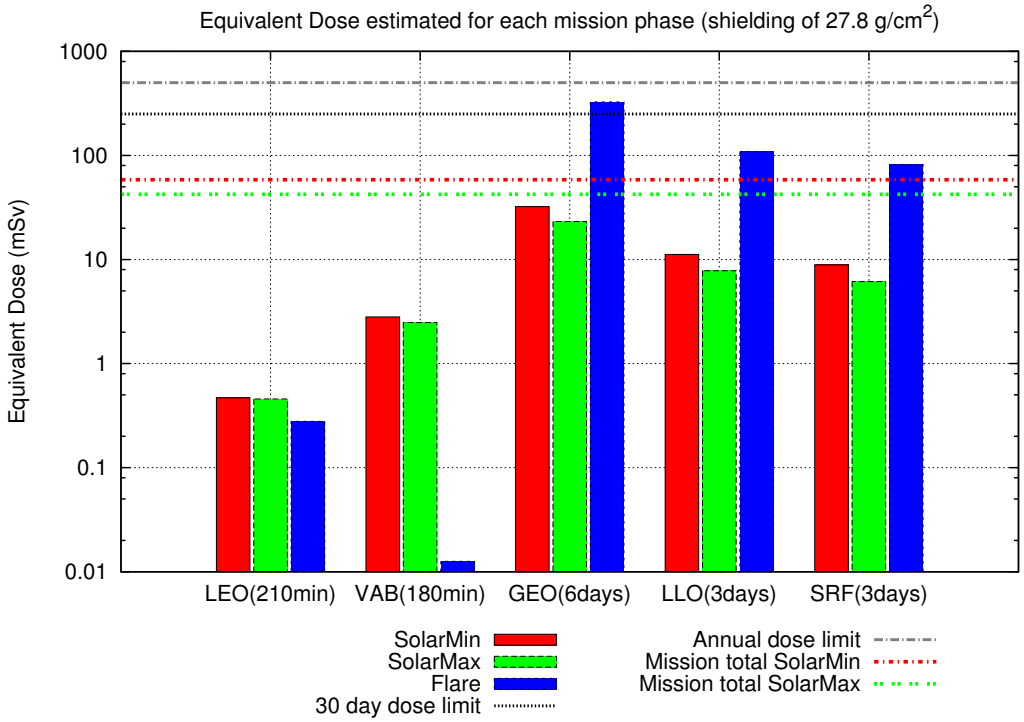

Figure 5.5: Equivalent dose for each weather scenario considering the total time of the mission under a shielding of 27,8 g/cm^2 of Aluminium (100mm). The horizontal lines indicate the total mission dose and the PEL in BFO.

In order to prevent excessive risks of radiation exposure a good planning of the mission timings could prove to be more efficient than increasing the depth of shielding in the spacecraft. Missions should be planned for periods of solar minimum activity, when flares are less likely to occur. Solar Flares however are not that predictable. Continuous observations of solar activity allow for the existence of flare alarms that give astronauts the possibility to refuge in areas of the spacecraft that provide more shielding. For future longer missions specially shielded areas in the spacecraft are being architected.

Chapter 6

Conclusion

The work presented in this thesis was mainly focused on the study of the radiation environment in space, its effects in astronaut crews and the development of a software tool (SRES) to systematize a way to simulate that environment taking as an example the case of a lunar mission. The SRES was entirely based on Geant4 and a set of control scripts in C++. The major details on its development were presented and a glimpse of its capabilities revealed in the assessment of dosimetric quantities. The simple spherical model used in the geometry of the simulation environment, as well as the methods of implementing the radiation incidence on the sphere, produced rather good results, in agreement with already existing values for dose in space. Equivalent doses of 55,5 mSv and 40,1 mSv were obtained for astronauts that embark in a lunar mission, during periods of solar minimum and solar maximum activity, respectively, considering a mission duration of 12 days. This values may vary up to 517 mSv if a large flare occurs during the mission.

It is important to note that all results obtained with SRES were based in fluence rates from CREME wich is not specifically designed for dose calculations and is more focused in the effects of radiation in micro-electronics. The approach used was to get from CREME only the fluence tables for the different locations and weather scenarios, all subsequent simulation an dosimetric calculations were entirely based in Geant4. SRES is still far from being a user friendly tool. Some improvements should be considered specially in what concerns to interface and data management. Also, as future work, it should be considered the use of fluence data from different sources such as Spenvis and ApexRad and the results compared to the ones obtained from CREME.

Appendix A

Integration Method

The CREME fluence rate data points table presents a variable bin width so that when the plots are presented in logarithmic scale, on the x axis, the bins look equally spaced.

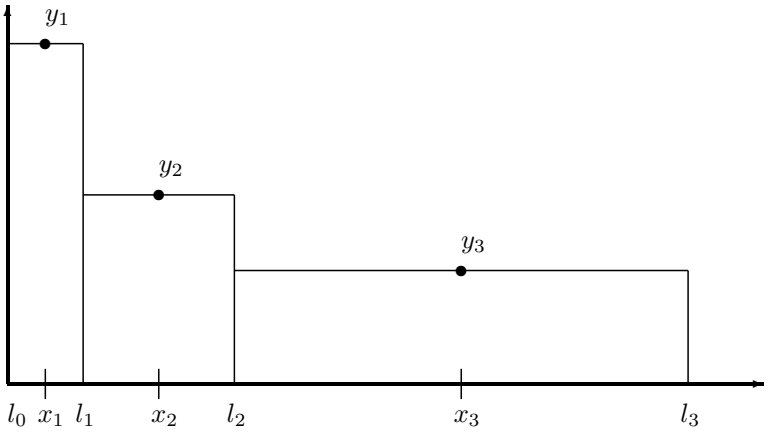

Since x points are presented equally spaced when the x axis is set to logarithmic scale, one must have:

$$log(x_{n+1}) - log(x_n) = c <=> log(\frac{x_{n+1}}{x_n}) = c <=> \frac{x_{n+1}}{x_n} = B^c \tag{A.1}$$

where B and c are constants and for simplicity I will call $B^c = a$. The points in CREME tables present $a = \frac{x_{n+1}}{x_n} = 1.013897396$.
Assuming that l_n is the upper limit of bin n and knowing that they also follow $l_n a = l_{n+1}$ we can write:

$$ax_n - l_n = al_n - ax_n \;\Leftrightarrow\; l_n = \frac{2x_n a}{a+1} \tag{A.2}$$

Now we can get the value of any l_n. For l_0 once you get l_1 simply do $l_0 = 2x_1 - l_1$

This way the width Δb of all bins comes:

$\Delta b_1 = l_1 - l_0$

$\Delta b_2 = l_2 - l_1$

$\Delta b_3 = l_3 - l_2$

...

$\Delta b_n = l_n - l_{n-1}$

And to integrate we simply need to multiply the bin width by the y_n values and sum for all n.

$f_n = y_n \ \Delta b_n$

$$\sum^{n} f_n = \text{Total intensity} \tag{A.3}$$

Bibliography

[1] Marc Heppener. Spaceward ho! *EMBO Reports*, 9:S4–S12, 2008. doi:10.1038/embor.2008.98.

[2] Review of U.S. Human Spaceflight Plans Committee. Seeking a human spaceflight program worthy of a great nation. Technical report, NASA, 2009.

[3] Alexander Anikeev. Manned astronautics - figures & facts. http://space.kursknet.ru/, July 2012.

[4] NASA PDS Geosciences Node. `http://pds-geosciences.wustl.edu/missions/chandrayaan1/default.htm`.

[5] William C. Feldman, Alan B. Binder, and Sylvestre Maurice. Lunar prospector reduced spectrometer data - special products. `http://geo.pds.nasa.gov/missions/lunarp/reduced_special.html`.

[6] NASA PDS Geosciences Node. `http://pds-geosciences.wustl.edu/missions/lro/default.htm`.

[7] ISRO. `http://www.chandrayaan-i.com/index.php/chandrayaan-2.html`.

[8] De Rosa. Characterisation of potential landing sites for the european space agency's lunar lander project. *43rd Lunar and Planetary Science Conference; Proceedings of the Conference.Woodlands, Texas*, 2012.

[9] European Science Foundation. Science-driven scenario for space exploration. 2008.

[10] Journal of the ICRU Vol 10 No 2 (2010) Report 84. Oxford University Press. doi:10.1093/jicru/ndq019.

[11] Journal of the ICRU Vol 11 No 1 (2011) Report 85. Oxford University Press. doi:10.1093/jicru/ndr011.

[12] ICRP, 2007. The 2007 Recommendations of the ICRP. ICRP Publication 103. Ann. ICRP 37 (2-4).

[13] Journal of the ICRU (1980) Report 33. Oxford University Press.

[14] Robert A. Braeunig. Orbital Mechanics. `http://www.braeunig.us/space/orbmech.htm`.

[15] NIST database. `http://physics.nist.gov/PhysRefData/IonEnergy/tblNew.html`.

[16] S.P. Swordy. The energy spectra and anisotropies of cosmic rays. *Space Science Reviews*, 99:85–94, 2001.

[17] Prantzos, N. On the origin and composition of galactic cosmic rays. *A&A*, 538:A80, 2012.

[18] National Research Council. *Managing Space Radiation Risk in the New Era of Space Exploration.* National Academies Press, Washington D.C., 2008.

[19] Journal of Geophysical Research, Vol. 111, A12211, 23 PP., 2006. doi:10.1029/2006JA011827.

[20] Journal of Geophysical Research, Vol. 68, NO. 3, P. 607, 1963. doi:10.1029/JZ068i003p00607.

[21] S. Maurice et al. High-energy neutrons from the moon. *Journal of Geophysical Research*, 105:20365–20375, 2000.

[22] Adams et al. The ionizing radiation environment on the moon. *Advances in space research*, 40:338–341, 2007.

[23] Anthony L. Turkevich. The average chemical composition of the lunar surface. *Proceedings of the Lunar Science Conference*, 4:1159–1168, 1973.

[24] USNRC Technical Training Center. *Reactor Concepts Manual.*, volume 09-Biological Effects of Radiation.

[25] Concurrent Design Facility. Near earth exploration minimum system assessment. CDF Study Report CDF-114(A), ESA, May 2011.

[26] G.Reitz. Biological effects of space radiation. *ESA Space Weather workshop proceedings*, 1998.

[27] NASA Langley Research Center. Apollo Expeditions to the Moon, Mission Profile. `http://www.hq.nasa.gov/office/pao/History/SP-350/profile.html`.

[28] Richard W. Orloff. *Apollo By The Numbers: A Statistical Reference.* NASA SP-2000-4029. NASA Headquarters - Washington, DC 20546, 2000 (Revised, September 2004). ISBN 0-16-050631-X `http://history.nasa.gov/SP-4029/Apollo_00a_Cover.htm`.

[29] Robert A. Braeunig. Apollo 11's Translunar Trajectory. `http://www.braeunig.us/apollo/apollo11-TLI.htm`.

[30] CREME site. `https://creme.isde.vanderbilt.edu/`.

[31] Geant4 website. `https://geant4.web.cern.ch/geant4/`.

[32] Wilmot N. Hess and Arthur J. Starnes. Measurement of the neutron flux in space. *Phys. Rev. Lett.*, 5:48–50, Jul 1960.

[33] NASA Human Spaceflight. `http://spaceflight.nasa.gov/shuttle/reference/shutref/structure/structure.html`.

[34] Metal Suppliers Online: Material Property Data. `http://www.suppliersonline.com/propertypages/2024.asp`.

[35] McIlwain, C. E. (1961), Coordinates for mapping the distribution of magnetically trapped particles, *J. Geophys. Res.*, 66(11), 3681–3691, doi:10.1029/JZ066i011p03681.

[36] Oleg Mazonka. Solid angle of conical surfaces, polyhedral cones, and intersecting spherical caps. *eprint arXiv:1205.1396*, 05/2012.

[37] Steve Koontz. Jon Progress in Spacecraft Environment Interactions III:The Role of Structural Shielding Mass in Avionics Performance in Single Event Effect Environments, *2007 Biennial Research Report*, Johnson Space Center.

[38] Benton EV, Henke RP, "Radiation exposures during space flight and their measurement" , Adv. Space Res. 1983; 3(8):171-85.

[39] Cucinotta FA, "Physical and biological organ dosimetry analysis for international space station astronauts". Radiat Res. 2008 Jul;170(1):127-38.

[40] Foelsche T. "Estimates of radiation doses in space on the basis of current data". Life Sci Space Res. 1963;1:48-94.

[41] Francis A. Cucinotta. Radiation risk acceptability and limitations.

[42] NIST website. `http://physics.nist.gov/PhysRefData/Star/Text/PSTAR.html`.